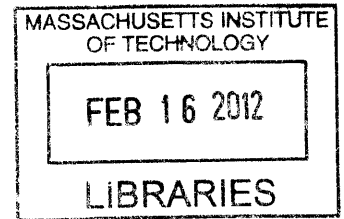


**Robot Design for Leak Detection in  
Water-Pipe Systems**

by  
Changrak Choi



Submitted to the Department of Mechanical Engineering  
in partial fulfillment of the requirements for the degree of

Master of Science in Mechanical Engineering

at the

MASSACHUSETTS INSTITUTE OF TECHNOLOGY

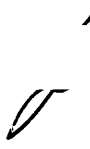
February 2012

© Massachusetts Institute of Technology 2012. All rights reserved.

Author .....

Department of Mechanical Engineering  
January 20, 2012

Certified by .....

 .....

Kamal Youcef-Toumi  
Professor of Mechanical Engineering  
Thesis Supervisor

Accepted by .....

 .....

David E. Hardt  
Chairman, Department Committee on Graduate Students



# **Robot Design for Leak Detection in Water-Pipe Systems**

by

**Changrak Choi**

Submitted to the Department of Mechanical Engineering  
on January 20, 2012, in partial fulfillment of the  
requirement for the degree of  
Master of Science in Mechanical Engineering

## **Abstract**

Leaks are major problem that occur in the water pipelines all around the world. Several reports indicate loss of around 20 to 30 percent of water in the distribution of water through water pipe systems. Such loss of water represents critical waste of valuable resources, especially in countries such as Saudi Arabia where water is scarce. Moreover, leaks provide pathways for outside contaminants to enter into water pipe system which can deteriorate the quality of water and pose health risks to those drink from it. Considering these negatives, the importance of detecting where the leaks occur within vast network of water pipe system cannot be overemphasized. Further, for accurate and effective detection of the leaks, an in-pipe approach is taken which differs from previous detection methods.

This thesis is on the design of mobile robotic platform that carries the necessary sensor and travels inside the water pipe systems. To begin with, experiments were carried out to investigate the suitability of using acoustic sensor to detect the leaks and favorable results were obtained. Then design specification of the mobile robotic platform that will carry the sensor is discussed with brief description of each components of the robot given. As components for the mobile robotic platform, a rigid-flexible robotic joint is developed that enables the robot to travel through bends and turns. Further, a novel braking mechanism using permanent magnet is presented. The mechanism results in a friction controllable leg that can be used to slow down and control the speed of robot in the presence of water flow. Finally, possible candidates for propulsion unit are discussed and evaluated with guidance for future work to be progressed.

Thesis Supervisor: Kamal Youcef-Toumi  
Title: Professor of Mechanical Engineering



## Acknowledgements

First of all, I would like to thank my supervisor, Professor Kamal Youcef-Toumi, for his valuable and kind advice, support, guidance and patience during my masters. Not only has he given me academic advices regarding the work, but also shown me kind support and encouragement to which I am truly grateful and feel deeply in-debt. Moreover, I would like to thank him for giving me the chance to participate in "*Clean Water and Clean Energy*" workshops held in Saudi Arabia for both years 2011 and 2012. It was great experience meeting with the collaborators and also wonderful opportunity to speak and become friends with colleagues working on different areas.

Secondly, I wish to thank all my lab mates, Mauricio Gutierrez, Sang-il Lee, Amith Somanath, Cynthia Panas, Andreas Schuh, Iman Soltani Bozchalooi, especially Dimitris Chatzigeorgiou and Marie Sacretes-Fleur for all the help and support they have given me in and out of the lab. In addition, I would like to thank Dr. Atia Khalifa, Dr. Rashed Ben Mansour for the advices throughout the work.

My deepest gratitude goes to my family for their endless love and support throughout my life; this thesis is simply impossible without them. Also, I would like to thank the King Fahd University of Petroleum and Minerals (KFUPM) in Dhahran, Saudi Arabia, for funding the research reported in this thesis through the *Center for Water and Clean Energy* at MIT and KFUPM. In addition, I would like to thank Korean Government for giving me the scholarship during the masters program.

Finally, I thank Seoha Min, my lovely fiancé and soon to be wife, for her constant love and for the happiness she has brought to my life.



# Contents

<b>1</b>	<b>Introduction</b>	<b>15</b>
1.1	Importance of Detecting Leaks . . . . .	15
1.2	Advantages of In-Pipe Approach . . . . .	16
1.3	Overview of the Thesis . . . . .	17
<b>2</b>	<b>Sensing Using Acoustic Sensor</b>	<b>19</b>
2.1	Abstract . . . . .	19
2.2	Introduction . . . . .	20
2.3	Experimental Setup . . . . .	23
2.4	Results and Discussion . . . . .	26
2.4.1	Acoustic waves with Flow . . . . .	28
2.4.2	Acoustic waves without Flow . . . . .	32
2.5	Conclusion . . . . .	35
<b>3</b>	<b>Overview of Mobile Robotic Platform</b>	<b>37</b>
3.1	Design Specifications . . . . .	37
3.1.1	Working Environment . . . . .	37

3.1.2	Requirements .....	38
3.1.3	Constraints .....	40
3.2	Existing In-pipe Robots for Inspection .....	41
3.3	Components of Mobile Robotic Platform .....	43
3.3.1	Sensor .....	43
3.3.2	Communication Device .....	44
3.3.3	Propulsion Unit .....	45
3.3.4	Braking Mechanism .....	45
3.3.5	Rigid-Flexible Joints .....	46
<b>4</b>	<b>Rigid-Flexible Robotic Joints</b> .....	<b>47</b>
4.1	Abstract .....	47
4.2	Introduction .....	47
4.3	Design of the Rigid-Flexible Joints .....	51
4.4	Manufacturing Process .....	53
4.5	Prototype .....	57
4.6	Experiments .....	58
4.6.1	Test for Bends .....	58
4.6.2	Test for Pressure .....	59
4.6.3	Test for Water-Proof .....	60
4.7	Conclusion .....	61



<b>5</b>	<b>Friction Controlling Mechanism Using Magnetic Force</b>	<b>63</b>
5.1	Abstract .....	63
5.2	Introduction .....	63
5.3	Overview of Mechanism .....	66
5.3.1	Description .....	68
5.3.2	Design Parameters .....	69
5.3.3	Generating a Controllable Normal Force .....	71
5.3.4	Cancellation and Reduction of Torque .....	73
5.4	Analysis of Forces and Effects of Design Parameters .....	75
5.4.1	Methods of Calculating Magnetic Force .....	75
5.4.2	Modeling of Magnet .....	77
5.4.3	Forces and Torques for Single Stator/Rotor Magnet .....	80
5.4.4	Forces and Torques for Multiple Stator/Rotor Magnets .....	83
5.5	Prototype as Proof of Concept .....	87
5.6	Discussion and Future Work .....	89
5.7	Conclusion .....	90
<b>6</b>	<b>Propulsion Unit</b>	<b>91</b>
6.1	Analysis of the Drag forces .....	91
6.2	Candidates for Propulsion Unit .....	94
6.3	Comparison of Different Propulsion Units .....	96
6.4	Conclusion .....	97

<b>7 Conclusion and Future Work</b>	<b>99</b>
<b>A Friction Controlling Mechanism</b>	<b>101</b>
A.1 Using Magnetic Force .....	101
A.2 Linkage or Cam Mechanism .....	103
A.2.1 Anti-Rotation Mechanism .....	105
A.3 Pneumatic / Hydraulic or Cable .....	106
<b>B Magneto-hydrodynamic Propulsion Unit</b>	<b>109</b>

# List of Figures

2-1	Test loop and control of hydrophone location. . . . .	25
2-2	Actual leak signal measured by the hydrophone at leak section, line pressure	26
2-3	Sample of noise generated by the source at 50 Hz measured 1-meter from the source in water, no flow-no pressure situation. . . . .	28
2-4	Effect of line pressure on signal attenuation at different frequencies and different locations from the source. . . . .	30
2-5	Measuring at 4 meters downstream the acoustic source. . . . .	32
3-1	Existing in-pipe robots from literature survey. . . . .	42
3-2	Candidates for the communication system. . . . .	44
4-1	Robotic platform with required modules put together. . . . .	48
4-2	Junctions at water pipe systems. . . . .	49
4-3	Concept of rigid-flexible robotic joints. . . . .	50
4-4	Discontinuity at the joints for an in-pipe robot and continuous shape of eel. . .	51
4-5	Flexible body with female and male mating parts. . . . .	52
4-6	Rigid-flexible joint put together. . . . .	52
4-7	Overall process for making rigid-flexible robotic joints. . . . .	53
4-8	CNC machined mold for flexible body made from machinable wax. . . . .	54

4-9	Male and female mating parts. . . . .	54
4-10	Male and female mating parts placed inside the mold. . . . .	55
4-11	First prototype of rigid-flexible joint. . . . .	57
4-12	Assembly of two rigid modules with rigid-flexible joint. . . . .	58
4-13	Rigid-flexible joint prototype traveling through the bends. . . . .	59
4-14	Pressure test for the cylindrical shape with hollow inside. . . . .	60
4-15	Cylindrical flexible body with cotton wool filled inside. . . . .	60
5-1	Examples of wheeled in-pipe robots with active friction varying mechanism. . . . .	65
5-2	Typical three bar linkage mechanism used to provide active friction force. . . . .	65
5-3	Overview of the mechanism. . . . .	66
5-4	Front view of the mechanism. . . . .	67
5-5	Side view of the mechanism. . . . .	67
5-6	Mechanism with different number of rotor magnets. . . . .	69
5-7	Mechanism with different number of stator magnets. . . . .	70
5-8	Configuration of stator/rotor magnet with angle $\theta$ . . . . .	71
5-9	Comparison of magnetic forces in front and rear stator/rotor pair. . . . .	73
5-10	Steps in modeling a magnet as equivalent magnetic charge. . . . .	77
5-11	Magnetic forces acting on typical stator/rotor configuration. . . . .	79
5-12	Forces and torques on single stator/rotor magnet. . . . .	80
5-13	Normal force and torque produced with single stator/rotor magnet. . . . .	82
5-14	Comparison of normal force produced for $N_r=N_s=3$ and 6. . . . .	84

5-15	Comparison of torque produced for $N_r=N_s=3$ and 6. ....	84
5-16	Effect of increasing stator magnets on torque. ....	85
5-17	Torque cancellation effect of rear pair of stator/rotor magnet set. ....	86
5-18	Prototype I with only front stator/rotor pair. ....	87
5-19	Prototype II with both front and rear stator/rotor pair. ....	88
6-1	Schematic of the robotic platform inside a pipe with flow. ....	91
6-2	Schematic of magneto-hydrodynamic propulsion unit. ....	94
6-3	Schematic of propeller as propulsion unit. ....	95
6-4	Fish-like motion propulsion. ....	95
6-5	Water-jet propulsion unit. ....	96
A-1	Sketch of friction controlling mechanism using magnetic force. ....	101
A-2	Sketch of linkage and cam mechanism to control friction. ....	103
A-3	Sketch of anti-rotation mechanism. ....	105
A-4	Sketch of mechanism using pneumatic or cable to control friction. ....	106
B-1	Prototype of simple magneto-hydrodynamic propulsion unit. ....	109
B-2	Magneto-hydrodynamic unit tested inside salty water. ....	110
B-3	Unit submerged inside salt water with 20V applied. ....	111

# List of Tables

4-1 Soft materials that can be used for flexible body. . . . . 56

6-1 Comparison of different propulsion units. . . . . 97

# Chapter 1

## Introduction

### 1.1 Importance of Detecting Leaks

The water supply is perhaps one of the most important infrastructures that form essential backbone of any city around the globe. Such water supply is made possible through a network of water pipe systems with pipelines stretching over several thousand kilometers. However, these water pipelines, once buried underground will gradually wear out through years of usage and may develop leaks over time. Surprisingly, the percentage of water lost due to leaks in the water pipe system is significantly higher than what people normally expect. Around 20 to 30 percent of the water is lost due to leaks in the pipelines in the process of transportation. Several different reports indicate values of water lost due to leaks of around 20 percent - 15 to 25 percent for USA municipals, 20 percent for Canadian water authorities, and 30 percent for the study conducted in Saudi Arabia.

These losses in the transportation of water mean a significant financial loss for any nation, especially in the country like Saudi Arabia where water is scarce and the cost of water per cubic meter is high. Further, the leaks lead to introduction of contaminants into the pipeline which could deteriorate the quality of water and give rise to health risk

for those drinking from it. Therefore, it is necessary to fix these leaks and first step in doing so is accurately identifying where the leaks are within the vast network of water pipe system.

## **1.2 Advantages of In-Pipe Approach**

Several methods exist that are employed by the water authorities to detect the location of the leaks. However, most of them are detecting leak from outside pipe system. The details of each method will not be discussed in the section, but the outside pipe approach has many limitations. First, there is problem of accuracy. Since the leaks are occurring at the pipe buried deep under the soil, the leak signal is greatly attenuated when it reaches the outer soil. This often leads to small leaks being undetected and sometimes the noise interference in between may result in false alarm. Further, most of outside pipe approach methods are affected by the ambient conditions such as pipe material, depth of soil, soil type, and even temperature. With so many ambient conditions influencing the result, it is hard to accurately locate the leaks and they often require manual work of skilled operators. Thus, most of outside pipe approaches are costly but not effective.

To more efficiently and accurately detect the leak, an in-pipe approach is taken. Here, a sensor that is used to detect the leak is mounted on a mobile robotic platform that travels inside the water pipe system. Having such mobile sensor inside the pipeline has great advantage as it largely eradicates the limitations of outside pipe approaches discussed above. Nevertheless, developing a mobile robotic platform to travel inside the



water pipe system is technically challenging and it is what this thesis is about, with special focus on the components that make up the mobile robotic platform.

### **1.3 Overview of the Thesis**

The overall thesis is presented as follow. In the chapter 2, experiments conducted using acoustic sensor to detect the leak is presented. From chapter 3 onwards, the focus is on the mobile robotic platform. Chapter 3 provides the overview of the mobile robotic platform by discussing the design specifications and giving brief explanation of each component. Chapter 4 outlines in detail the rigid-flexible robotic joint developed to enable the robot to travel through the junctions. Chapter 5 presents the work on a braking mechanism that uses permanent magnet to vary the friction force applied on the robot legs. Chapter 6 shows the propulsion unit to be developed for the mobile robotic platform and Chapter 7 concludes with consideration for the future work to be done.



# Chapter 2

## Sensing Using Acoustic Sensor

### 2.1 Abstract

This chapter presents experimental observations on the characteristics of the acoustic signal propagation and attenuation inside water-filled pipes. An acoustic source (exciter) is mounted on the internal pipe wall, at a fixed location, and produces a tonal sound to simulate a leak noise with controlled frequency and amplitude, under different flow conditions. A hydrophone is aligned with the pipe centerline and can be re-positioned to capture the acoustic signal at different locations. Results showed that the wave attenuation depends on the source frequency and the line pressure. High frequency signals get attenuated more with increasing distance from the source. The optimum location to place the hydrophone for capturing the acoustic signal is not at the vicinity of source location. The optimum location also depends on the frequency and line pressure. It was also observed that the attenuation of the acoustic waves is higher in more flexible pipes like PVC ones.

## 2.2 Introduction

Effective and efficient transportation of water from utility to consumer is critical. Addressing water losses during distribution could limit the need to access new sources of freshwater; which are already diminishing. Various experimental techniques using field tests for leak detection have been reported (1 and 2). The most commonly used method for detecting leaks in water distribution systems involves using sonic leak-detection equipment, which identifies the sound of water escaping a pipe. Methods based on detecting and further processing acoustic signals inside and outside pipes are prevalent in leak detection. Slightly more sophisticated over direct sound measurements methods are acoustic correlation methods where two sensors are used. The leak should be located between the two sensors and the time lag between the acoustic signals detected by the two sensors is used to detect and locate the leak (3). The cross-correlation method works well in metal pipes; however, the effectiveness of the method is not so reliable with plastic pipes.

The acoustic leak detection technique based on external measurements is normally faced by some serious challenges (4 and 5). The leak signal has low frequency contents (<50 Hz) and is highly attenuated in plastic pipes, greater attenuation in large diameter pipes, attenuation caused by soft soils; e.g. clay or grass, pipes buried under a water table level, and pipes with pressure less than one bar. This means that distances between the sensors and the type and quality of sensor are of great importance. Attempts to characterize leaks in pipelines by utilizing internal measurements of the acoustic signal generated by the leak were conducted using either a tethered hydrophone (6) or a free

swimming hydrophone (7).

The technique of in-pipe acoustic measurements relies mainly on the sound traveling through the water column inside the pipe. It is apparent that sound velocity in water pipes depends upon and is influenced by the pipe material or the elasticity modulus and the ratio between diameter and wall thickness (8). That is, larger diameters and more flexible pipes tend to attenuate higher frequencies. Accordingly, low-frequency signals will be more dominant. This effect makes leak signals susceptible to interference from low-frequency vibrations, e.g., from pumps and road traffic.

An experimental and theoretical investigation of the low-frequency acoustic propagation and attenuation characteristics of a submerged plastic water pipe was done by (9 and 10). Complex wave numbers were determined, which encompass both the wave speed and the wave attenuation. The wave speed for the in-vacuo pipe was found to be reduced substantially from the free-field value due to the pipe wall flexibility; when the pipe was submerged, this value was reduced yet further by the mass-loading of the pipe by the surrounding water. The measured attenuation was found to fluctuate but the average value compared well with the prediction. For the buried pipe, there was good agreement between the measured and predicted wave speeds, again, particularly at low frequencies. The surrounding soil markedly increases the wave attenuation compared with the in-vacuo case, which suggests an additional difficulty in that the signal to noise ratio will be substantially reduced.

An analytical model to predict the cross correlation function of leak signals in buried plastic water pipes, by combining the correlation technique with wave propagation

theory in plastic pipes, was developed (11). The model is based on a theoretical formulation of wave propagation in a fluid-filled pipe in-vacuo and the assumption that the leak sound, at source, has a flat spectrum over the bandwidth of interest. This model has been applied to explain some of the main features of experimental data, including wave propagation and attenuation. It has been shown that in the noise-free case, good levels of correlation are only possible for ratios of sensor distances from the leak of less than about 10 and that an estimate of the signal-to-noise ratio at a measurement position can be simply determined from the ratio of the peak values of the experimental result of the correlation coefficient and its corresponding theoretical prediction.

Recently, a lot of research is being considered on the approach of in-pipe measurements for leak detection. Being inside the pipe provides good opportunities for leak detection like being close to the leak itself and being less dependent on the background noise, pipe material, soil type, and environmental effects. On the other hand, many challenges and questions arise when using this approach like what to measure or what type of sensor (acoustic, pressure,...etc.) to be used inside the pipe? What is the leak effect on the measured parameter? What is the effect of flow conditions (line pressure, flow rate, etc.) of leak signal? Where to place the sensor with respect to the leak? And so on.

The objective of the present work is to experimentally acquire the fundamental knowledge of how an acoustic wave emitted from a leak propagates and attenuates inside a plastic water-filled pipe under different pipeline conditions, using in-pipe acoustic measurements. The leak frequency and location of the leak are simulated by an acoustic

source of known location, frequency, and amplitude. It is a fundamental study yet it is very important for designing a good in-pipe acoustic leak detection system.

## **2.3 Experimental Setup**

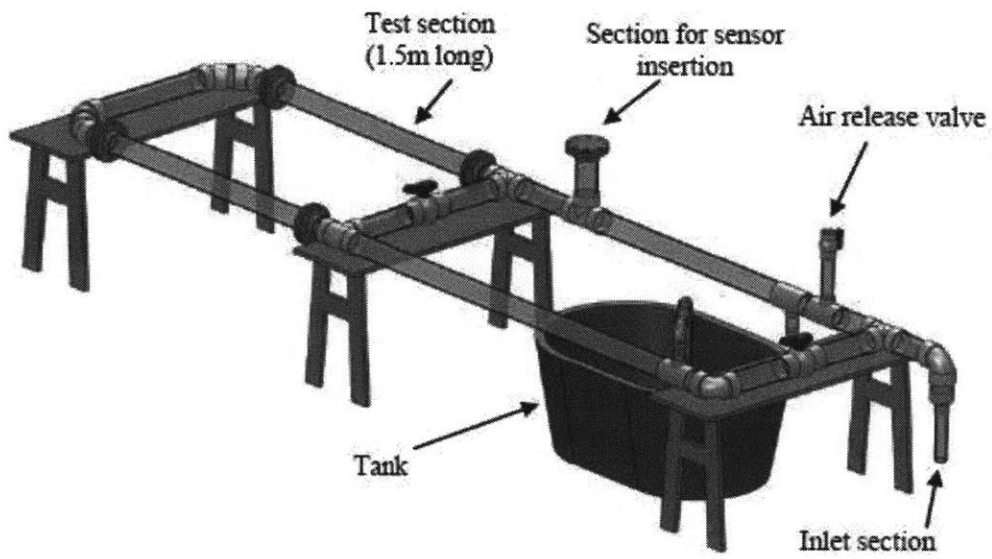
Two Laboratory setups were used for testing the propagation and attenuation of an acoustic wave:

(1) A water closed loop, shown in Figure 2-1a, to simulate the water distribution network under different flow conditions. It consists of a 4-inch acrylic pipe loop with a total length of 14 m. The loop inlet can be connected to the municipality water supply by a hose or to a 10 hp centrifugal pump. Water is circulated using a large tank. The loop is fitted by flow control valves to operate at different conditions of pressures and flow rates. The setup also allows having stagnant water (no flow situation) at different pressures. It also allows different water flow rates/pressures when using the pump. A pressure gage is installed on the pipe for measuring the line pressure. An acoustic source (exciter connected to audio amplifier) is attached to the internal wall of a 4-inch pipe, at a fixed location, and produces a tonal sound to simulate the leak noise. The magnitude and frequency of the source was adjusted from a source generator/amplifier system. A hydrophone moves at the pipe centerline and captures the signal at different distances from the acoustic source. Data are collected at high rates and analyzed using an FFT algorithm.

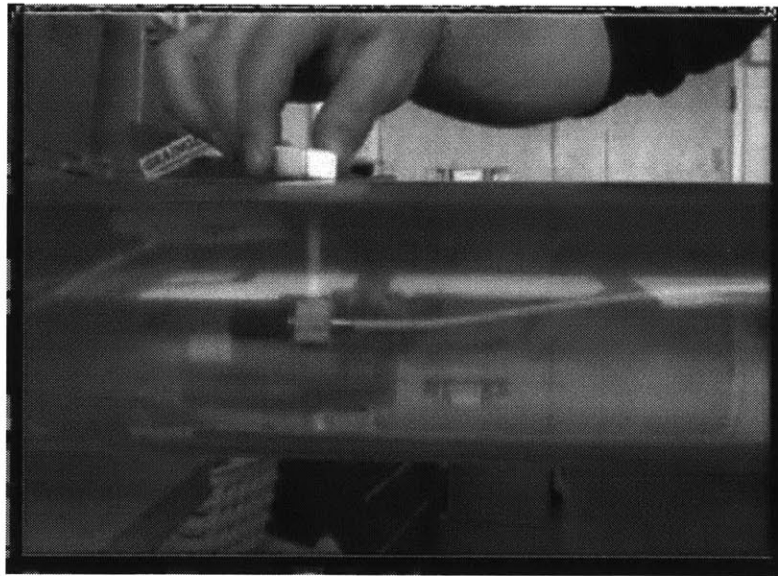
(2) A simple straight PVC, SCH 80, pipe (6 m long) with a closed end. The acoustic source is attached to the closed end of the pipe and water is supplied from the open end. A hydrophone is used to receive the acoustic signal inside the pipe at different location. There is no water flow with this setup, only the water pressure and the frequency of the acoustic source can be controlled.

The hydrophone, B&K model 8103 with sensitivity  $25.9 \mu\text{V}/\text{Pa}$ , is inserted into the pipe through a capped tee with sealant for the hydrophone cable. It is placed at the pipe centerline by a small plastic holder which is made mobile by magnets to move inside the pipe with respect to the acoustic source as shown in Figure 2-1b. A charge to voltage DeltaTron® converter is connected in series with the hydrophone and the sensor is powered from the DeltaTron® WB 1372 module. The output of the later module is then connected to a power amplifier and signal conditioner from Stanford Research Systems (Model number SR560). The unit has variable gain with low, high, and band-pass filter capabilities. The outputs of both hydrophone and pressure transducer are directed to a NI 9234 module on a cRIO-9113 reconfigurable chassis using a cRIO-9022 real-time controller. The sampling rate can be selected manually by the user and can go up to 51.2 KHz.





(a) A schematic of the test loop



(b) Hydrophone location with respect to the source is controlled by external magnet

Figure 2-1: Test loop and control of hydrophone location.

## 2.4 Results and Discussion

To give an idea about the acoustic signal of actual leak when measured from inside the pipe, stagnant water at a pressure of 250 kPa is allowed to leak from the 100 mm pipe to air from a hole of 6 mm in the pipe wall. The hydrophone is placed at the pipe centerline at the leak section (50 mm from the leak hole, pipe radius). Figure 2-2 shows the frequency spectrum of the hydrophone signal. A peak frequency is shown close to 105 Hz and few side bands appeared at different frequencies. Compared to the no leak signal (closed hole) which shows no peaks, these peaks represent the signature of the leak. However, it is not easy to follow the leak signal with real flow since the flow turbulence overcomes the leak wave. Thus simulating the leak using acoustic tonal source with controlled range of frequency and amplitude will hopefully provide more information about the acoustic wave propagation inside the water pipelines.

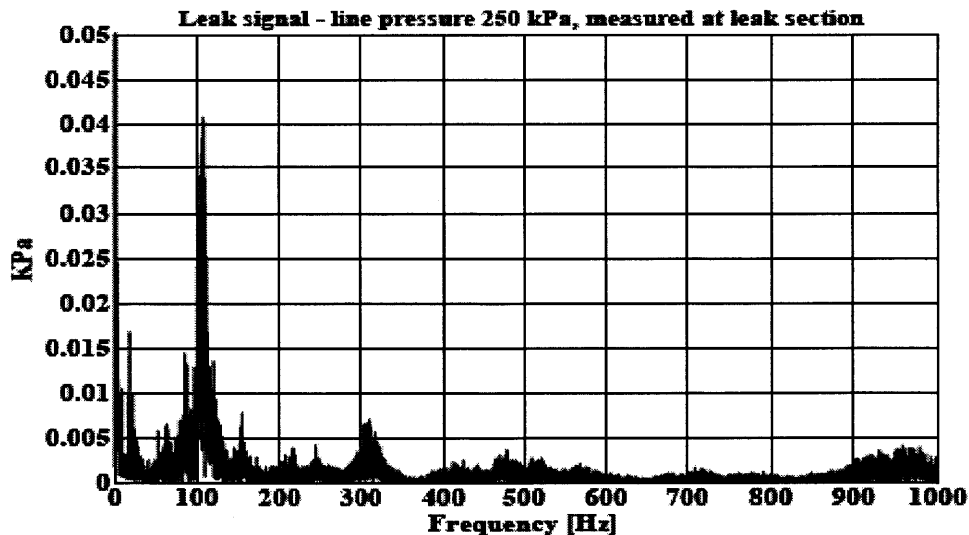


Figure 2-2: Actual leak signal measured by the hydrophone at leak section, line pressure is 250 kPa and no water flow.

The acoustic source used in experiments is an exciter, with audio amplifier, used to generate tonal noise at the required frequency with the help of tone generator software. The hydrophone location with respect to the acoustic source can be changed from outside the pipe. Data collected are analyzed using FFT algorithm. The FFT represents the signal strength at frequency range of interest and is a good tool when the signal is generated under the conditions of pipe flow. Figure 2-3 shows a sample of noise generated by the source at 50 Hz and measured 1 m from the source in water at no flow, no pressure situation. The same signal was recorded at 1 meter from the leak at both sides. The FFT magnitude (the peak value) of the generated signal at the specific frequency is used to assess the attenuation of the acoustic wave inside the pipe. One may observe the difference in the FFT magnitude between the actual leak signal and the generated signal, y-axis in figures 2-2 and 2-3. Controlling the wave amplitude is very helpful with real pipe flow.

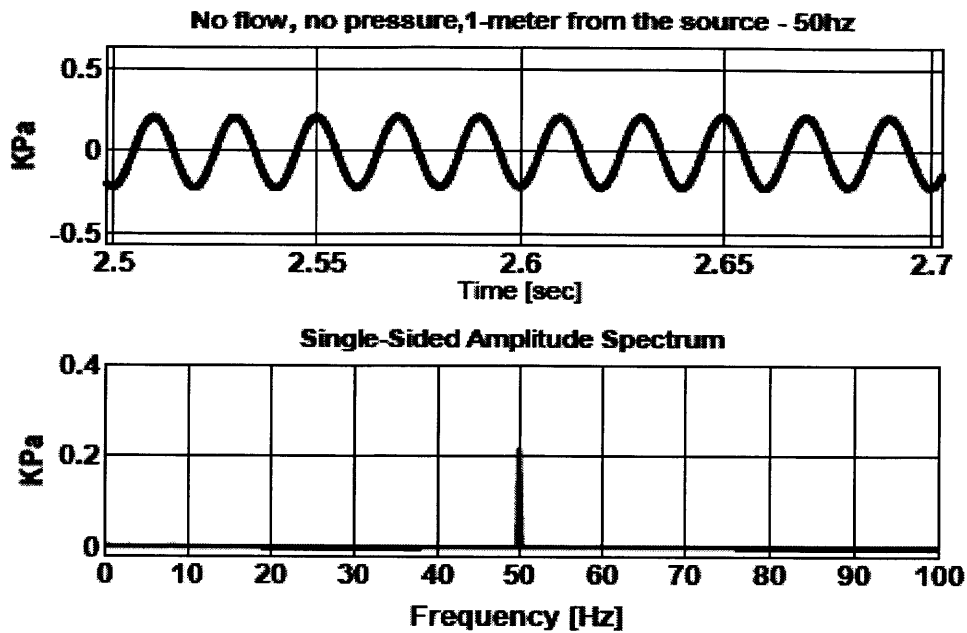
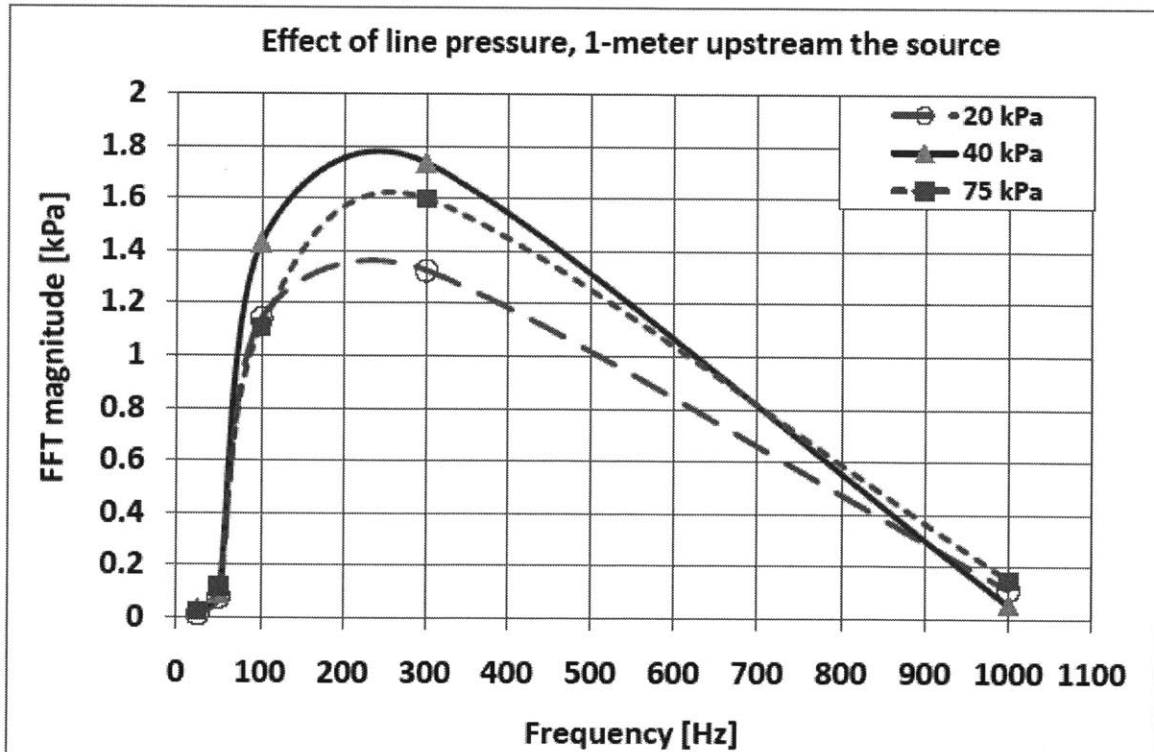
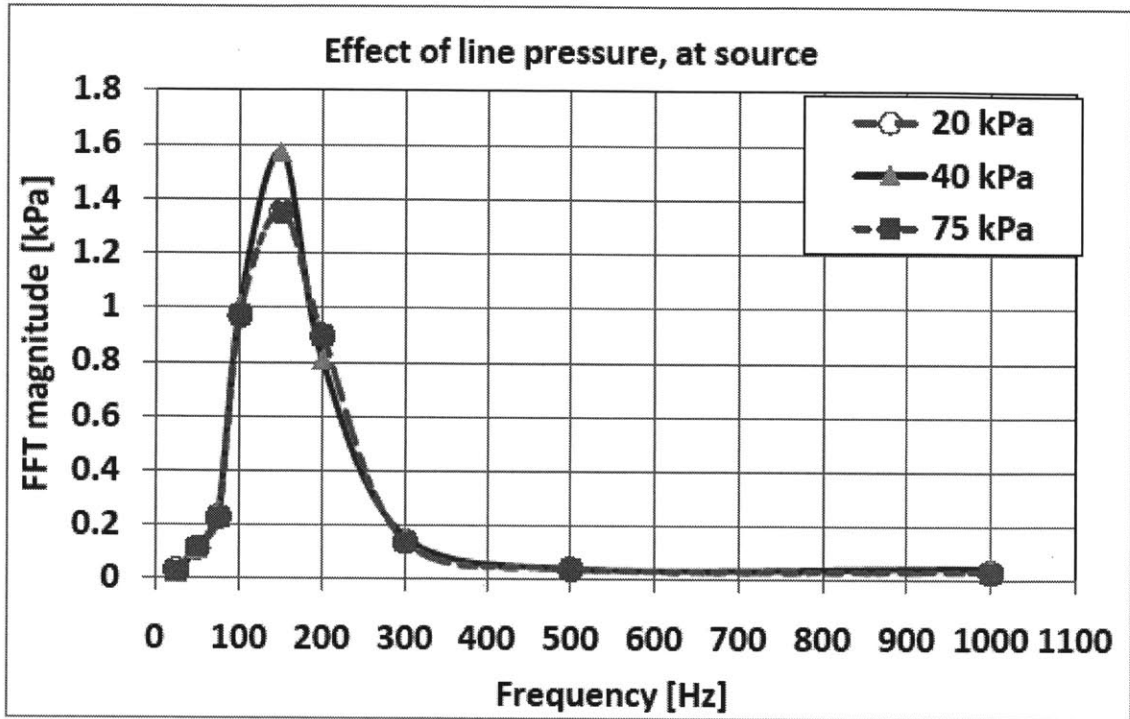


Figure 2-3: Sample of noise generated by the source at 50 Hz measured 1-meter from the source in water, no flow-no pressure situation.

### 2.4.1 Acoustic waves with Flow

In this section, results are presented for the experiments carried out using the 4-inch acrylic tube water loop with the pump used to circulate the water. By controlling the pump speed, flow is created at different rates and pressures, namely, flow speeds of 0.5, 0.82, and 1.15 m/s are achieved corresponding to pressures of 20, 40, and 75 kPa; respectively. A set of acoustic waves having frequencies between 25 Hz and 1000 Hz is examined under these flow conditions. The receiver hydrophone is placed at different locations with respect to acoustic source. Figures 2-4 (a, b, and c) show the results of this experiment.



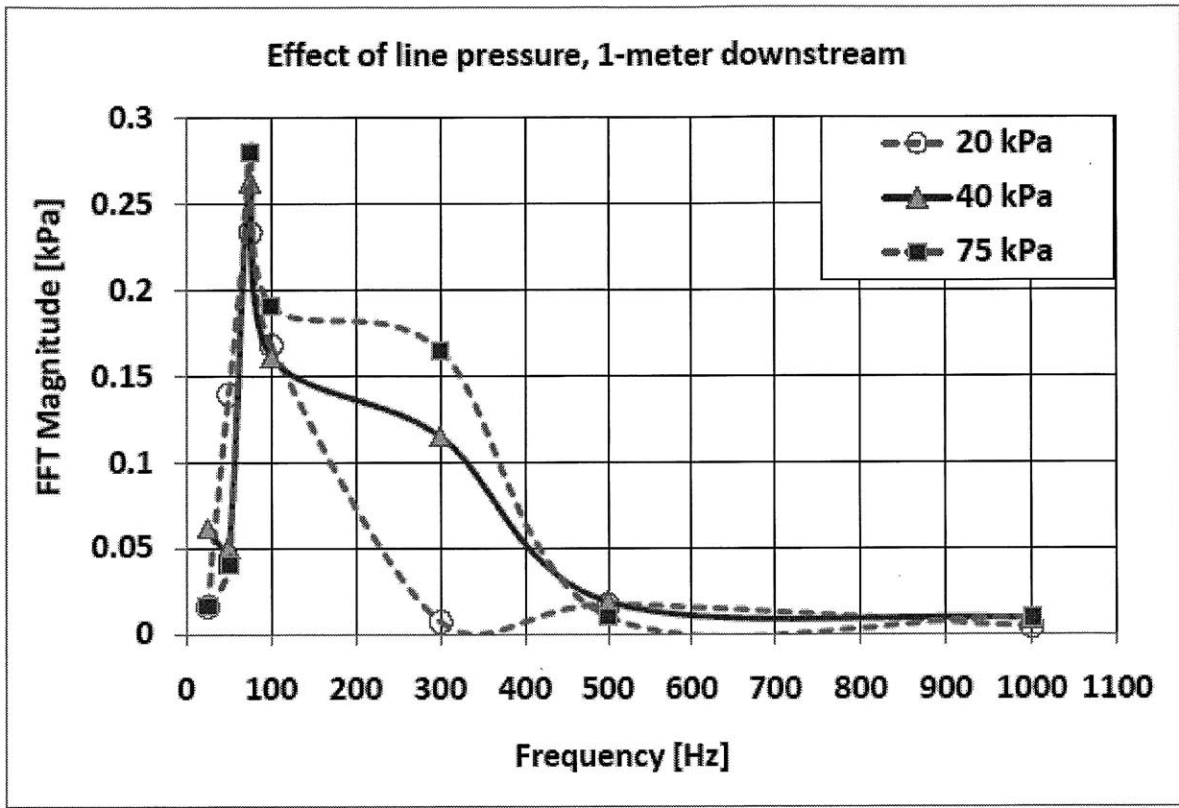


Figure 2-4: Effect of line pressure on signal attenuation at different frequencies and different locations from the source.

Figure 2-4a, the hydrophone was located at the acoustic source section. In Figure 2-4b, the hydrophone is located 1-meter upstream the source. In Figure 2-4c, the hydrophone is located 1-meter downstream the source. For each generated signal, the peak value of the signal frequency in the spectrum is considered for comparison (values on the y-axis). The amplitude of the generated signals is kept constant. It should be mentioned here that other frequencies appear in the spectrum due to flow turbulence.

The figures reveal interesting observations. For the tested range of pressure, the

strength of signals with frequencies approximately between 75 to 300 Hz is well captured by the hydrophone. Line pressure of 40 kPa corresponds to the best readings in this range of frequency. Results are showing that the strength of the signal measured 1-meter upstream is much higher than the same signal measured 1-meter downstream. It is even comparable (or better) to the signal measured at the source location. This observation proves that there is an interaction between the propagating wave and the flow direction in water-filled pipes; practically since similar signal were recorded previously at 1 meter upstream and downstream the leak in the case of no pipe flow. The authors believe that this point needs more analytical and experimental investigations in future.

To have more insights on the effect of signal frequency, the hydrophone was located 4-meters downstream the acoustic source. Frequencies from 25 to 1000 Hz were generated under line pressure of 75 kPa and results are shown in Figure 2-5. Two peaks were found at 75-100 Hz and 500 Hz. It appears that different frequencies propagate and attenuate differently with distance. Examining the FFT values on the y-axis for figures 2-4 and 2-5 reveals the fact that the wave is attenuated with distance downstream from the source. In general the attenuation is higher for high frequency signals.

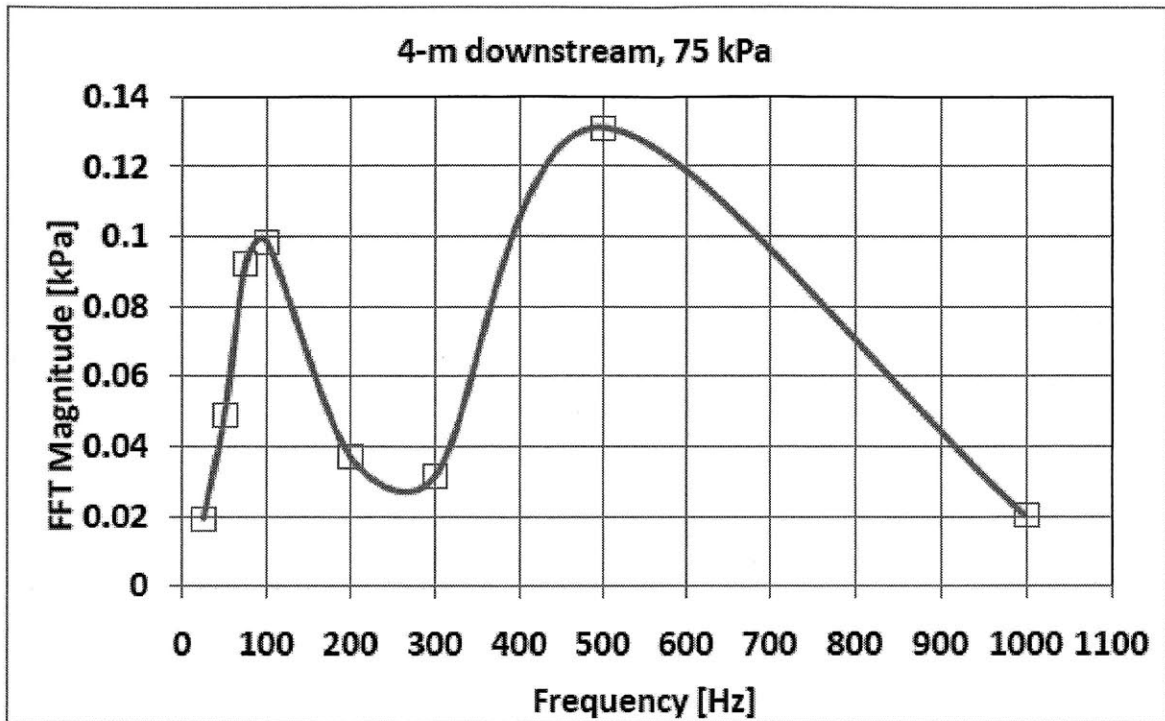


Figure 2-5: Measuring at 4 meters downstream the acoustic source

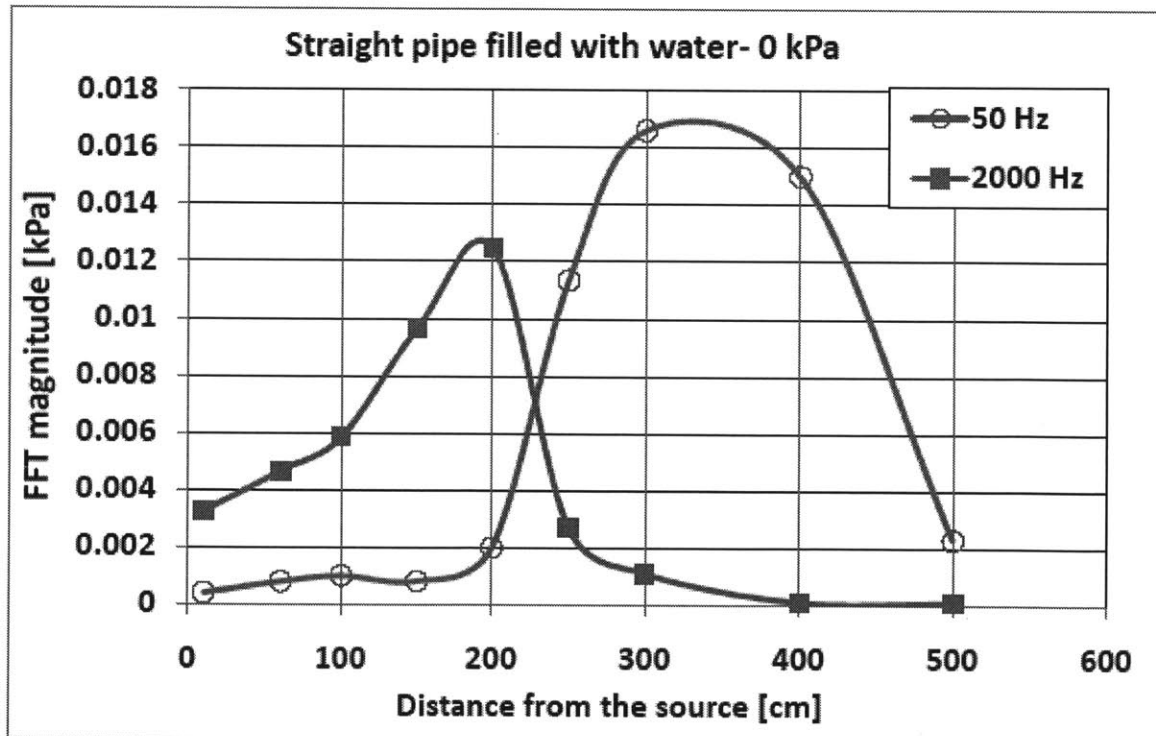
## 2.4.2 Acoustic waves without Flow

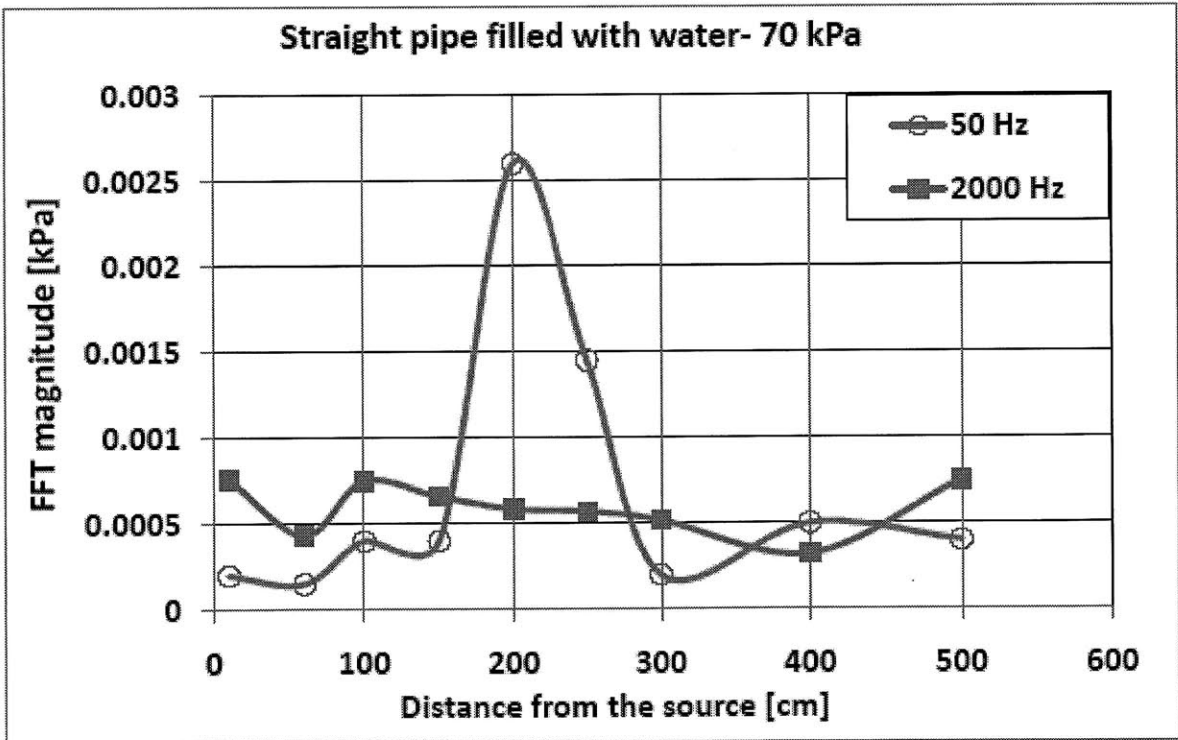
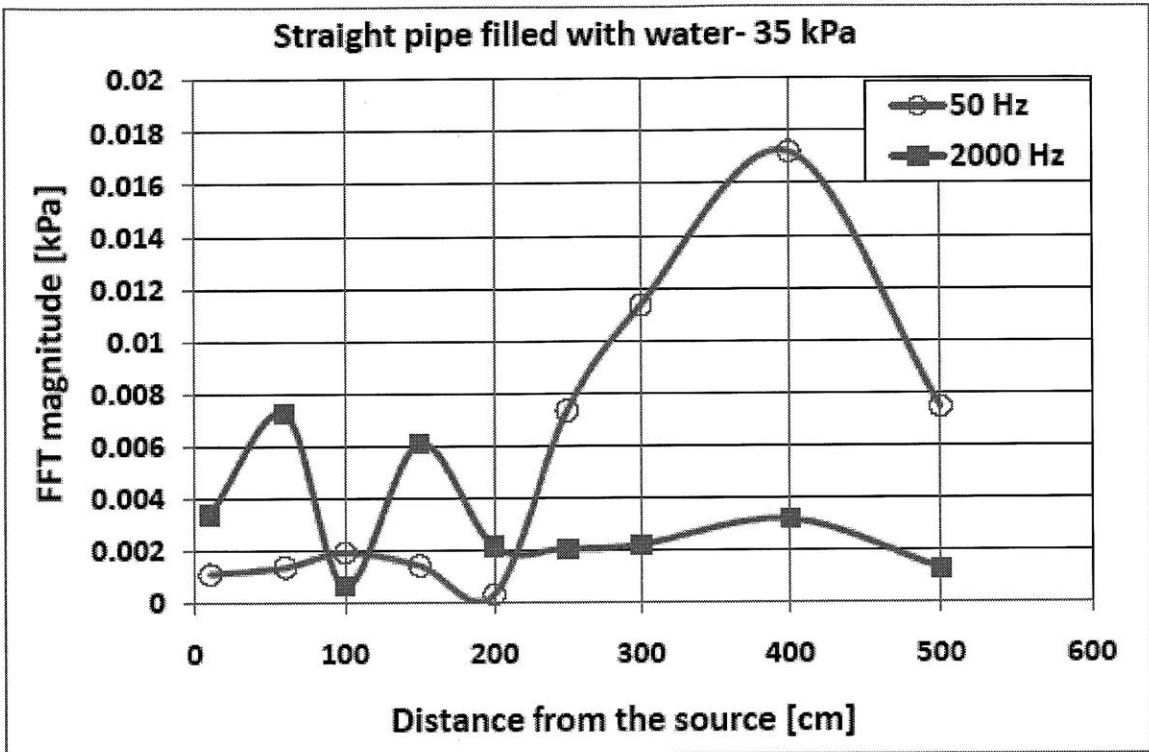
In this section, a 6-meter straight PVC pipe is used to pressurize the water under stagnation (no flow) conditions. One end is closed with a cap flange and the acoustic source is mounted on this end cap inside the pipe. Water is pressurized from the other end. The hydrophone is inserted from a capped tee close to the water supply end and moves along the pipe centerline to receive the acoustic signal at different location. The goal of this setup is to compare the signal attenuation in the PVC pipe with those previously measured using the acrylic tubes using the simple network geometry of straight pipe. Acrylic tubes are more rigid and fragile. Low and high frequency samples of 50 and 2000



Hz are shown in Figure 2-5 at different value of water pressure inside the PVC pipe.

The first important result from Figure 2-6 is that the peak value is not at the acoustic source. This simply means that placing the sensor at the source location (at leak location) may not be the optimum location to capture a good clean signal. For the case of 0 kPa, Figure 2-5a, the low and high frequencies peak at different distances from the source. High frequency signal attenuates very fast with increasing the pressure; while the low frequency signals still able to peak at a longer distance from the source. Even with the same frequency of 50 Hz, the location and magnitude of the peak depend on the line pressure.





Comparing the values of the FFT magnitudes in Figure 2-6 with those presented in Figure 2-4, one can realize that the big attenuation in the acoustic signal is due to the pipe material. The PVC pipe is more flexible and absorbs the energy of the propagating wave. Thus, detecting leaks in plastic PVC pipes is not an easy task.

## **2.5 Conclusion**

Results showed that the low frequency acoustic signals behave differently from high frequency ones. High frequency signals get attenuated quickly with increasing distance from the source. Attenuation is less for low frequency components, practically from 100-400 Hz at low pressures. The line pressure has a clear effect on the wave propagation at high frequency inside the pipe. Optimum location for the sensor to acquire good clean signal with respect to low frequency acoustic source is estimated to be 2 to 4 meters for the no flow situation. This distance depends on the source frequency and line pressure. Many reflections were measured when the sensor is located exactly at the leak section. Hydrophone directionality inside the pipe is a parameter to be considered. The attenuation of the acoustic waves is higher in more flexible pipes. In the case of real pipe flow, it was found that placing the sensor upstream is better in capturing the acoustic wave. This conclusion may help in designing a good system for detecting leaks in water pipe networks.

These results may be different for different experimental setup, and more experimental work using different configurations is needed. Nevertheless the presented findings give some interesting information on the wave propagation in water-filled pipe.



# Chapter 3

## Overview of Mobile Robotic Platform

### 3.1. Design Specifications

The in-pipe approach taken as the solution of the leak detection problem within water pipe systems requires a mobile robotic platform to carry onboard sensors, communication system, and data processing unit. While carrying these instruments, the mobile robotic platform must be able to travel inside the water pipe system in both with and without flow as well as deal with the turns at the bends. To come up with viable design of such robotic platform, it is necessary to identify the design specifications that include working environment, requirements and constraints. The following is the list of such specifications.

#### 3.1.1 Working Environment

The mobile robotic platform is targeted for 4 inch diameter pipe. The reason for this is because the water pipe system consists mostly of 4 inch diameter pipes. Also, the water flow in such pipeline can vary from no flow to maximum flow rate of 2 m/s. The water becomes almost stagnant during the night when there is no water usage and becomes high

during the day when water demand is large. The pressure inside the water pipe can go up to 50 psi so the robotic platform must be able to withstand such pressure. In addition, there are junctions in the pipe system with maximum bend of 90 degrees for T-junctions. These and other information of the working environment is listed below.

- Water-pipe diameter = 4"
- Water flow velocity = 0 – 2 m/s
- Water pressure = Maximum pressure = 50 psi
- Water temperature = 5 – 30 °C
- Water pipe has junctions (maximum angle turn = 90 degrees (T-junction))
- Pipe material = PVC
- Flow medium = water
- Pipe wall may not be smooth due to clogging of substances (optional)

These points regarding working environment will have to be taken into consideration when it comes to robot design.

### **3.1.2 Requirements**

While working inside the environment described above, the mobile robotic platform has to meet certain requirements in terms of mobility to successfully carry out the task. To begin with, the robot has to travel stably at the centerline inside the pipe. This is to ensure

that the sensors are held in stable and fixed position relative to the pipe wall so that they can better detect the leak. In terms of speed, the robot can travel with the flow when the water inside the pipe flows quickly. Nevertheless, there comes times when the water is near stagnant. In such situation, the robot has to be able to propel itself forward through propulsion unit to a speed at least 0.2 m/s to effectively scan through the pipeline for leak. In addition, when the robot is flowing with the flow, it is desirable to be able to slow down or even completely stop if necessary. This might occur when the robot needs to make a turn or when the sensor indicates possible leak, thereby wants to take more sample data nearby. Also, while traveling through the pipeline, the robot has to be able to negotiate the turn of at most 90 degrees in the case of T-junction.

Besides the requirement for the mobility, the robotic platform must carry different modules onboard namely, sensor, communication device, data processing unit, and power source. Furthermore, it is desirable that the robotic platform has long operational hour which can immensely extended if a energy harvesting unit is implemented that will gather energy from water flow inside. Also, if possible, it is desirable for the robot design to have scalability. The following is the list of requirements described above.

- Able to travel stably at the centerline inside the water-pipe.
- Able to propel forward at least 0.2 m/s (even without flow)
- Able to slow down to desired velocity anywhere between 0m/s to  $V_{\text{flow}}$  (even with max. flow of 2 m/s) for sufficient time interval

- Able to stop completely without consuming power (optional – for energy harvesting)
- Able to travel against the flow (optional – not required)
- Able to turn at the junctions to desired direction (Max turn angle = 90 degrees)
- Able to carry different modules (sensor, communication devices, processing board, power source) of maximum 2kg load.
- Have long operational hour (optional – requires energy harvesting to recharge the power source)
- Scalability (optional - better to be scalable to larger pipe, even better to work in larger pipe dimension with same robot)

### **3.1.3 Constraints**

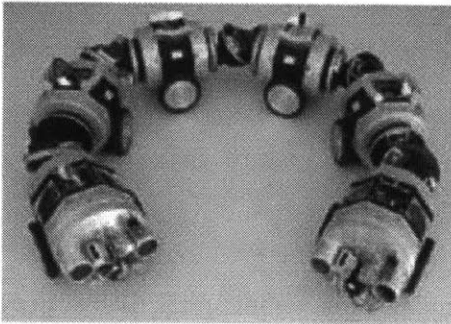
The biggest constraint for the mobile robotic platform comes from the fact that it is working inside the water supply pipe system. The first constraint is that all the component has to be on-board without any tethered component. The second is that the robotic platform should not produce any contamination inside the water pipe.

- All the components have to be on-board (On-board power, On-board controller, no external connection)
- No contamination to the water inside the pipe.



### 3.2 Existing In-pipe Robots for Inspection

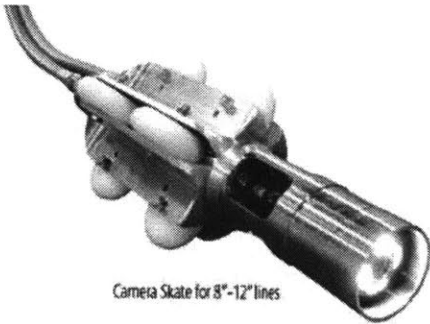
There are a number of good literature review papers on the in-pipe robots and 'Robotic Devices for Water Main In-Pipe Inspection: A Survey' [1] among others is a recently written paper that gives a comprehensive review of the existing in-pipe robots.



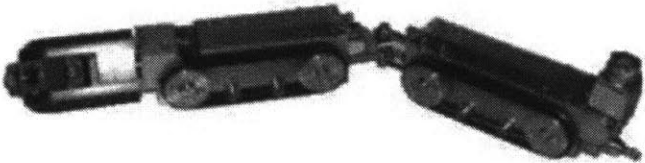
a) Makro



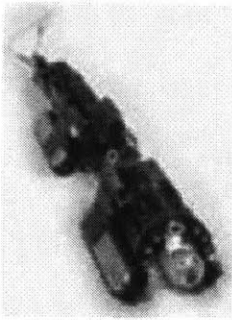
b) FR-150



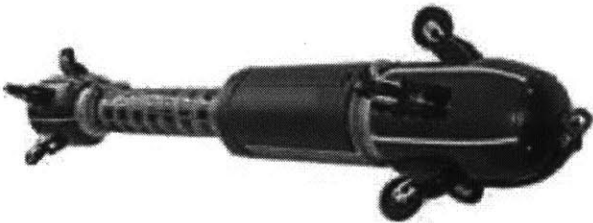
c) Pipe-Hunter



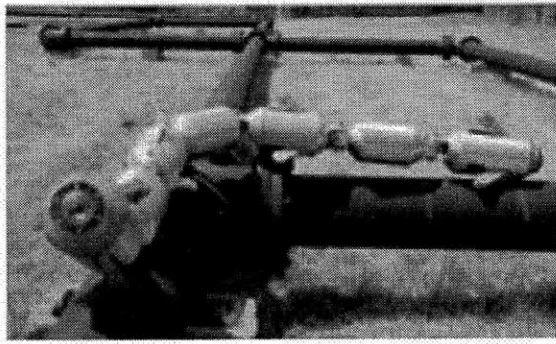
d) KFW 100



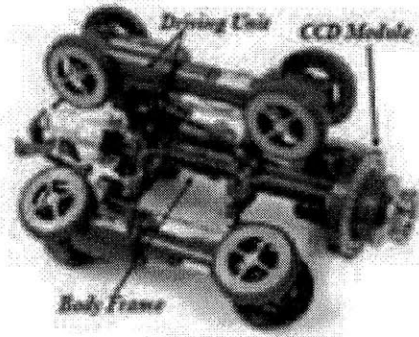
e) Versatrax 300



f) PipeScanner



g) Explorer



h) MrInspect

Figure 3-1: Existing in-pipe robots from literature survey

Figure 3-1 shows pictures of different in-pipe robots that were previously developed. Since the literature paper already discussed in detail about each in-pipe robots, instead of repeating the same, only overall comment with respect to the mobile robotic platform will be made in this section.

First, none of the previously developed in-pipe robots is designed to work inside the pressured liquid pipeline. All of them were targeted for use inside the gas pipeline where drag force is not a significant concern. However, for the mobile robotic platform, drag plays critical role since the density of water is about 3 orders of magnitude higher than that of air. Second, most of the in-pipe robots use wheel to drive the robot forward. This seems to be only practical and efficient solution for traveling inside a gas pipe. Nevertheless, for the application inside a water pipe, a propulsion unit based on propeller or water-jet can also be considered as an alternative to wheeled mechanism and might prove to be more effective. Last but not least, only few of the in-pipe robots developed so far is autonomous and un-tethered. For our purpose, it has to be autonomous and un-

tethered as the cost of inserting and retrieving the robotic platform from and out of water pipe systems is high. Thus, although there are a number of previously designed in-pipe robots, coming up with robot that works inside pressured water pipe system poses a new challenge and different approach to be taken.

### **3.3 Components of Mobile Robotic Platform**

There are five major components that consists the mobile robotic platform. The first is sensing module. They are sensor, communication device, propulsion unit, braking mechanism, and rigid-flexible joints.

#### **3.3.1 Sensor**

Sensor is a highly important component of the mobile robotic platform as it is the unit that actually detects the leak. In the previous chapter, an experiment using hydrophone (acoustic sensor) is presented and the result discussed. The acoustic sensing seemed to be promising as there is clear characteristic signal visible in the frequency domain in the case of leak which can be identified. Nevertheless, it becomes hard to identify such characteristic signal of the leak when there is high speed flow. This is due to additional noise created by the turbulence of the flow.

Going in a different direction, a sensor based on the localized pressure difference that occurs across the leak is now being investigated. This method is promised to work

for both flow and without flow and has shown to be effective means of detecting the leak. Nevertheless, the details of such pressure based sensor will be discussed in this thesis.

### 3.3.2 Communication Device

Communication device that will transmit the data gathered from the sensor is essential part of the robot. However, this communication device has to have a very strong transitivity as it will have to send data out from inside the water pipe system to outside the soil. That is through water, pipe wall, and 2-3m of sand soil.

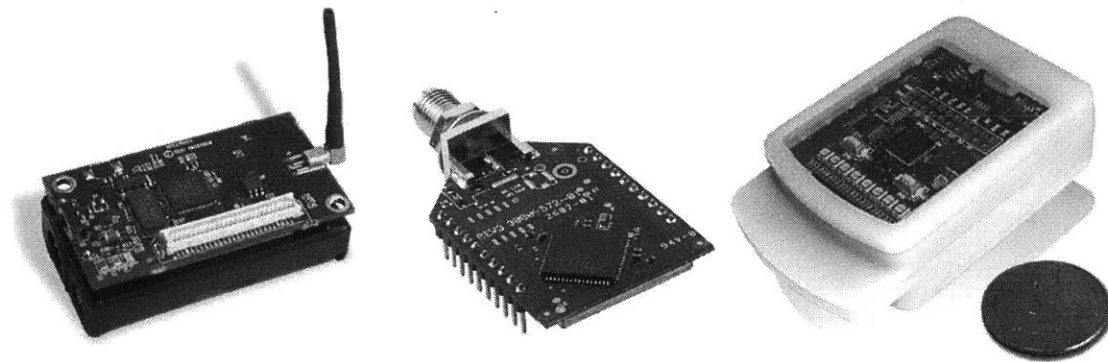


Figure 3-2: Candidates for the communication system.

Figure 3-2 shows MICA mote, Digi XBee Pro and SunSPOT system that were among the systems considered for the communication device. Discussion into the mobile platform is out of the scope for this thesis and will not be discussed further in detail.

### **3.3.3 Propulsion Unit**

Propulsion unit that will drive the mobile robotic platform around the pipe system is necessary when there is not enough water flow to push the robot forward. In the case of existing in-pipe robots for inspection, most of them make use of motor driven wheels to drive the system forward. However, this is because these in-pipe robots are designed to work inside the gas-pipe systems. The mobile robot platform differs in that it works inside liquid pipe system, and thus has to take into account of the different environment to come up with propulsion system that is most suitable. Chapter 6 will discuss about the propulsion unit in details.

### **3.3.4 Braking Mechanism**

When there is a sufficient flow inside the water pipe system, the robot will be pushed by the flow and follow the flow to travel inside the water pipe system. Nevertheless, there are times when it is necessary to slow down or even completely stop the robot in the presence of water flow. When the sensor reading indicates a possibility of the leak nearby, the robot will need to slow down to take more sample data to be more precise as to whether there is a leak in vicinity. Also, when making a turn at the junctions, the speed of the robot may have to be reduced to allow enough time for robot to bend and make a correct turn. Moreover, the robot may have to completely stop if it is to harvest energy from the water flow inside the pipe system and this preferably without consuming any energy. For these purposes, a braking mechanism becomes important part of the mobile robot platform and is discussed further in-depth in Chapter 5.

### **3.3.5 Rigid-Flexible Joints**

One of the requirements of the robot is to be able to onboard the different modules including sensor, communication, propulsion, braking unit, and power supply. As the diameter of the pipe is only 4 inch, incorporating all these components leads to the robot becoming lengthy similar to snake like robot. The problem rises in that a long rigid robot will not be able to turn at the junctions. A rigid-flexible joints is developed that will maintain the continuous shape of the robot while enabling it to turn at the junctions. The details of the rigid-flexible joint are presented in Chapter 4.

## **Chapter 4.**

# **Rigid-Flexible Robotic Joints**

### **4.1 Abstract**

In this chapter, a newly developed rigid-flexible robotic joint is discussed in detail. The concept of rigid-flexible robotic joint is presented and design of the prototype is given as a solidwork model. Then the manufacturing process for making the rigid-flexible robotic joint is shown with each steps in the fabrication highlighted. Finally, first prototype of the rigid-flexible robotic joint is presented and experiments that were carried out to validate the working of the joint are also described with results.

### **4.2 Introduction**

The mobile robotic platform that is developed to travel inside the water pipe system and detect a leak requires several modules to be incorporated into the system. First, a sensor has to be present that will gather data to identify a possible leak. Also, a communication

device needs to be placed inside that will send out the either raw or processed data to outside the water pipe system. If the sensor data requires certain processing, an additional processing unit too will have to be embedded. Further, a propulsion unit, braking mechanism with onboard power supply are needed to perform the necessary mobility functions to travel inside the pipe systems.

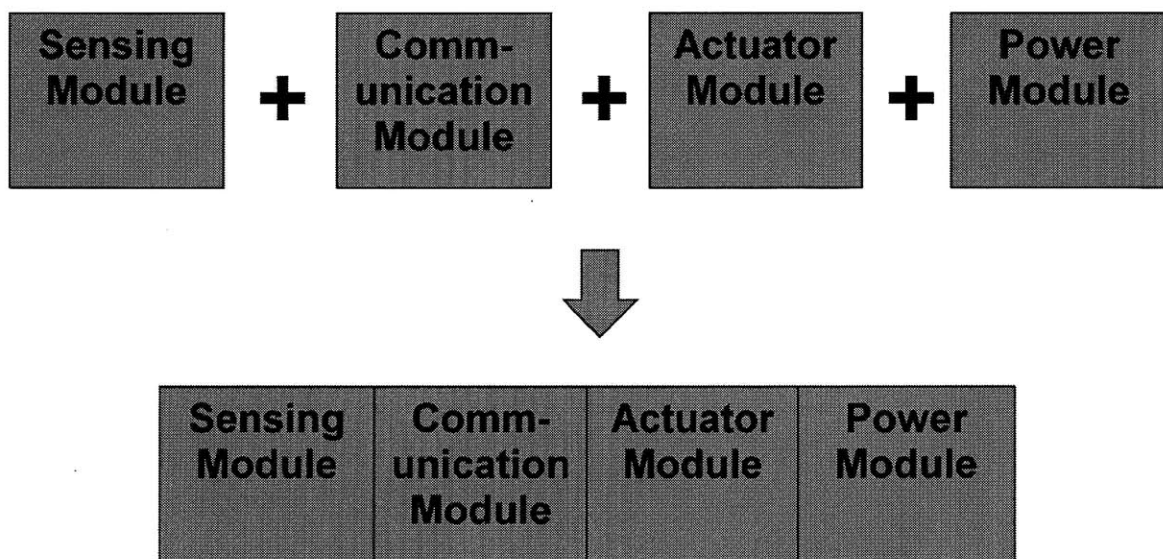


Figure 4-1: Robotic platform with required modules put together.

The constraints lie in the fact that the mobile robotic platform that has to incorporate all these components must fit inside 4 inch diameter pipe. Since it is desirable to have the robot blocking only partial fraction of the pipe, it places further constrain on the maximum diameter of the robot, preferably to about 2.5 inch in diameter. Hence, when all the required components is placed together, the robot will inevitably become lengthy similar to snake like robots as shown in Figure 4-1.



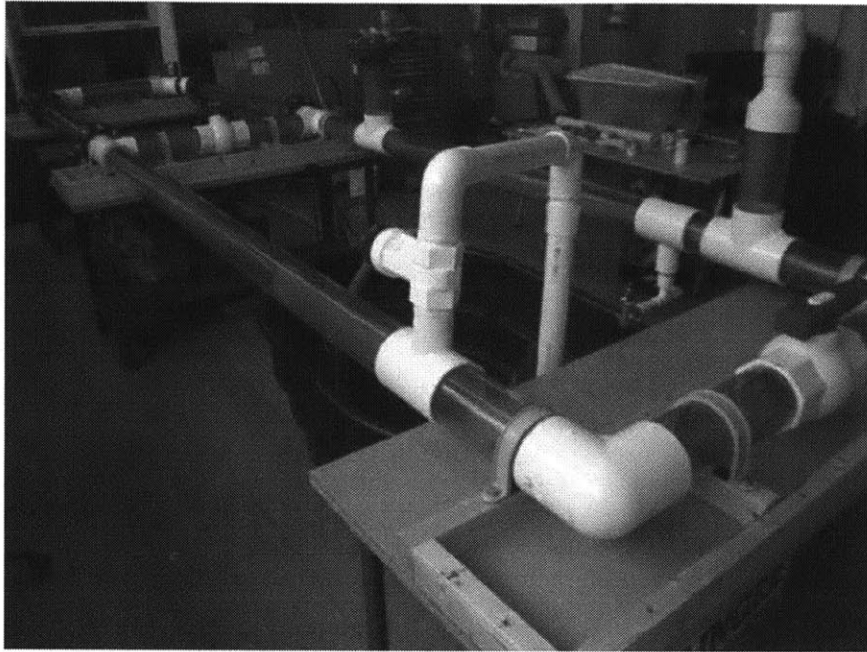


Figure 4-2: Junctions at water pipe systems.

The length of the robot becomes problematic when it has to negotiate the turns in the water pipe system. Figure 4-2 shows experimental setup that is used for sensor testing that exemplifies a typical water pipe system. As one can see, a water pipe system has many bends, most y-junctions and t-junctions that have maximum of 90 degrees bend. A lengthy rigid robot will not be able to go through these turns and this places a critical criterion on the maximum length that a rigid robot can have.

Therefore, a concept of rigid-flexible robotic joint is developed to enable the robotic platform to negotiate with the turns at the same time be sufficiently lengthy to incorporated all the required modules. Figure 4-3 shows the diagram that explains the concept of rigid-flexible robotic joints. Here the idea is to have each rigid module connected to each other by a flexible joint.

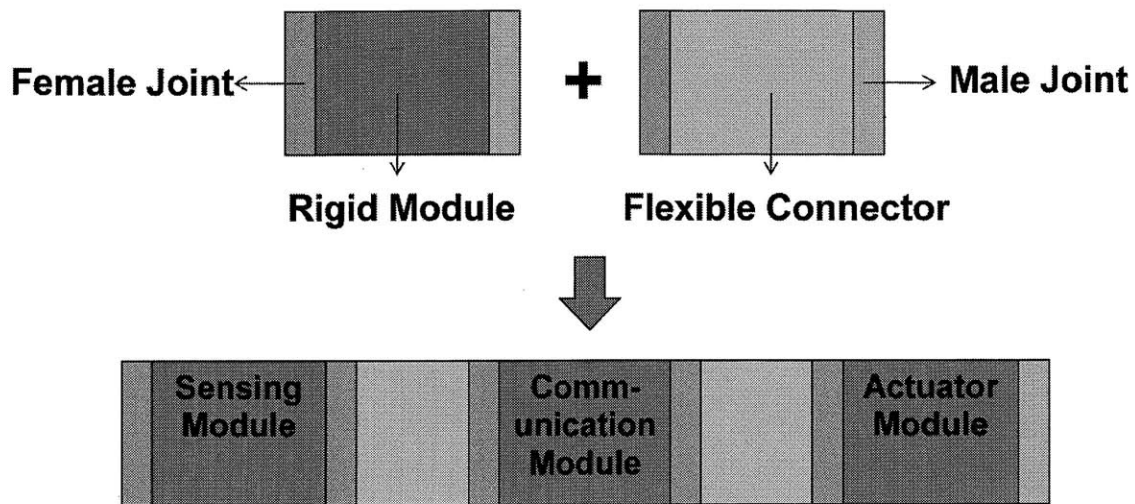


Figure 4-3: Concept of rigid-flexible robotic joints

In the literature, many of the existing in-pipe robots and snake like robots do have joints that connect different modules to deal with the turns. However, this concept of rigid-flexible joint differs from them for two main reasons. First, it provides continuous shape of the robot. Most of the existing joints are such that the at every joint, there is discontinuity of the overall robot shape. Figure 4-4 shows Explorer, a typical in-pipe robot built for inspection purpose. As you can see, the joints connecting the modules introduce a discontinuity in shape of the overall robot. Such discontinuity may not be problematic in case of gas pipe inspection robot. However, for the robotic platform that travels inside water pipe system, the discontinuous shape will greatly increase the overall drag coefficient of the robot. This will lead to greater induced drag to overcome when the robot needs to slow or stop in the presence of high flow. The rigid-flexible robotic joint concept proposed here can provide an overall continuous shape similar to an eel in Figure 4-4 which brings down the drag coefficient to a very small value.

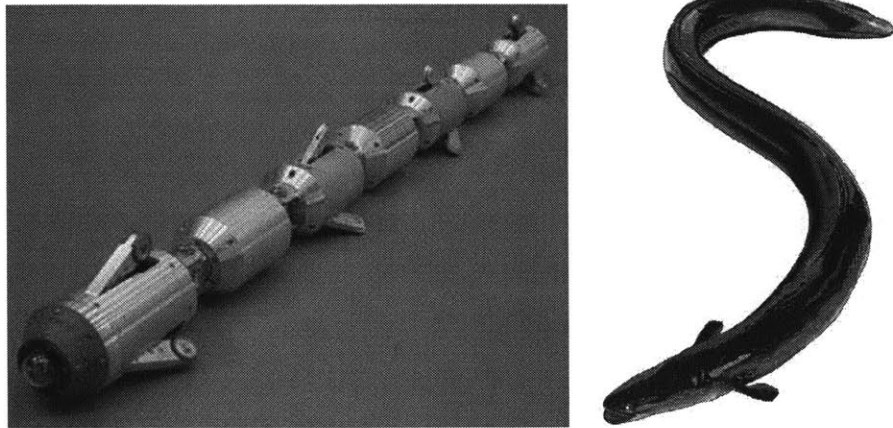


Figure 4-4: Discontinuity at the joints for an in-pipe robot and continuous shape of eel.

The second advantage is that any electronics, actuators, sensors can be embedded in the space of flexible joints. The existing joints for in-pipe robots only functions as a joint that can bend. However, the rigid-flexible robotic joint developed here can have electronics placed inside and thus provide functions to the robotic platform in addition to acting as a bending joint.

### **4.3 Design of the Rigid-Flexible Joints**

Figure 4-5 shows the prototype solidwork design of rigid-flexible joint. The flexible part consists of flexible cylindrical body with male and female mating part attached to each ends. The flexible cylindrical body can be made from various soft materials that include silicon rubber, silicone gel and polyurethane. The male and female mating part attached to flexible body is held in place by the adhesion property of the soft material on the surface as well as undercut in the mating part that is held by soft material.

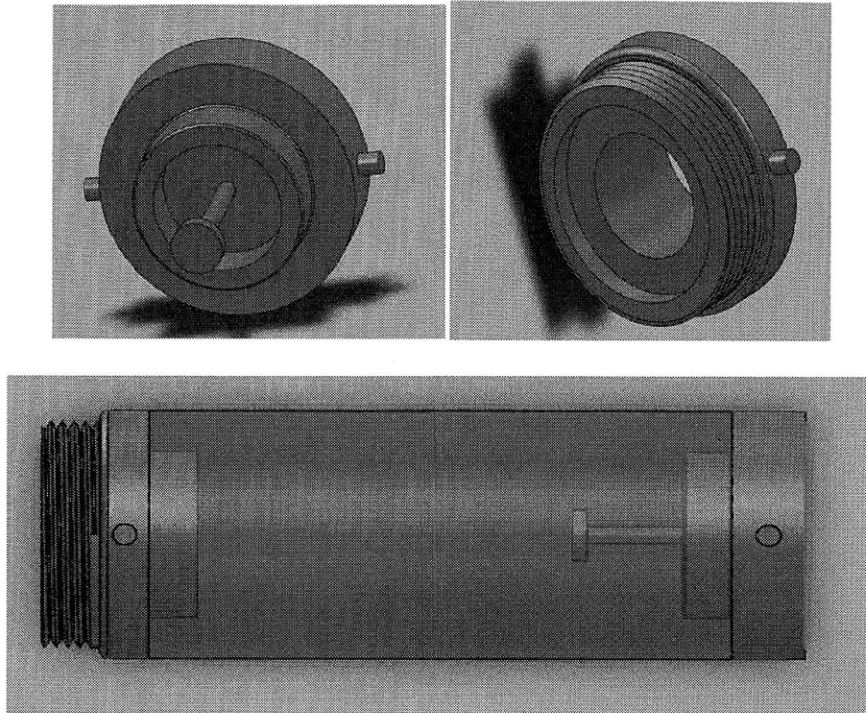


Figure 4-5: Flexible body with female and male mating parts.

Figure 4-6 shows the rigid-flexible joint connecting two rigid modules. The rigid module too have male and female mating parts is used to attached and detach itself from the rigid-flexible joints. This allows for modular approach to the building the robotic platform.

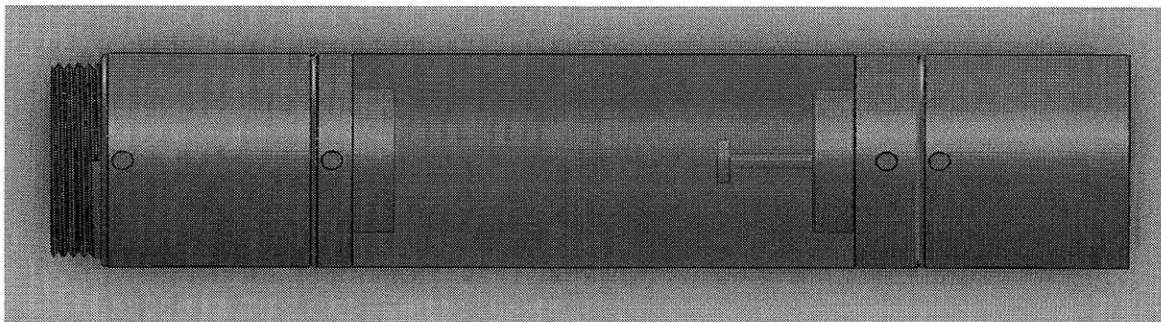


Figure 4-6: Rigid-flexible joint put together.

## 4.4 Manufacturing Process

Figure 4-7 shows the overall manufacturing process for the rigid-flexible robotic joint.

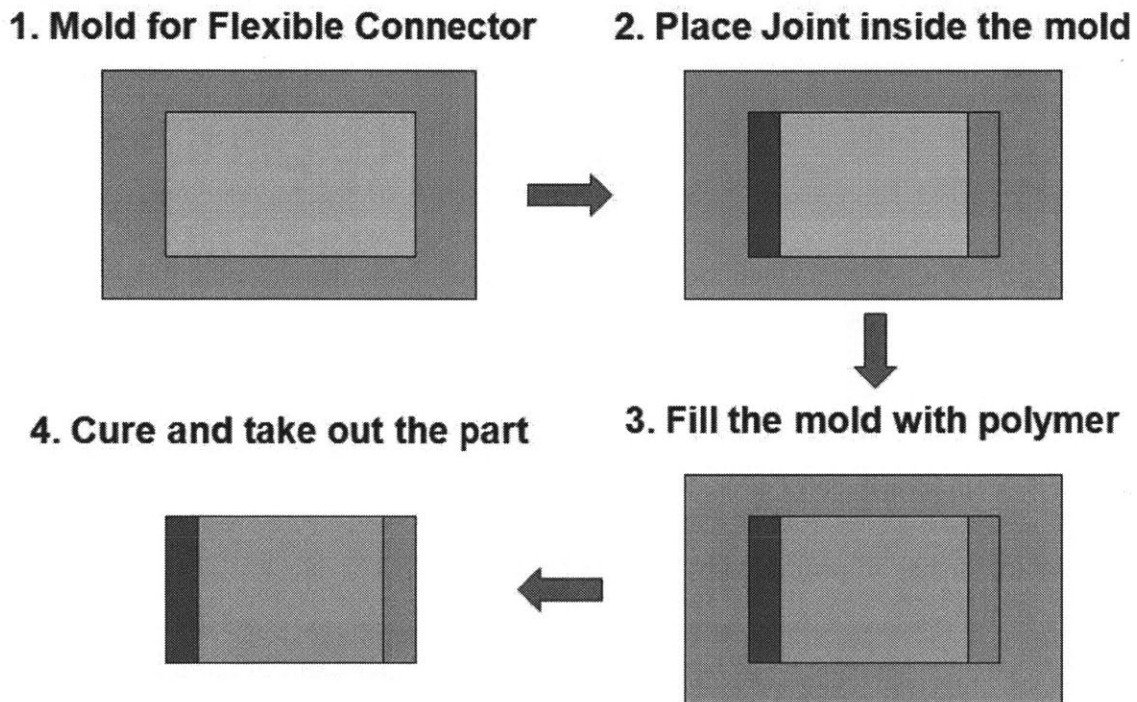


Figure 4-7: Overall process for making rigid-flexible robotic joints.

The first step in fabricating rigid-flexible joint is to make a mold for the flexible body. The mold is made from machinable wax and the shape of the mold is machined using CNC machine. For the robotic platform, the shape of flexible body is cylindrical but it can be altered to take on any arbitrary shape for other various purposes. Figure 4-8 shows the CNC machined mold that is used to make the first prototype.

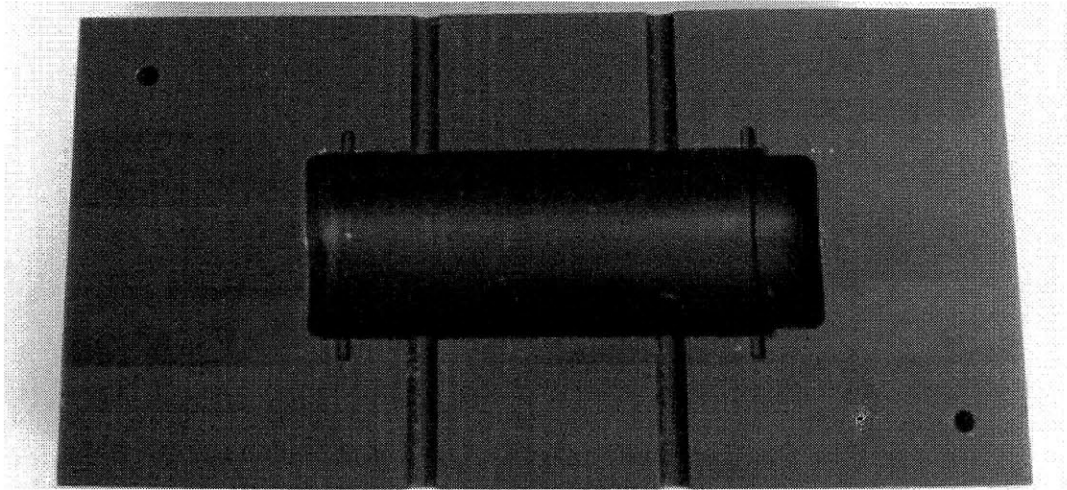


Figure 4-8: CNC machined mold for flexible body made from machinable wax.

Second step is to make the male and female mating parts that will be attached to the flexible body. Figure 4-9 shows the male and female mating part that has been manufactured using 3d printer with ABS material.

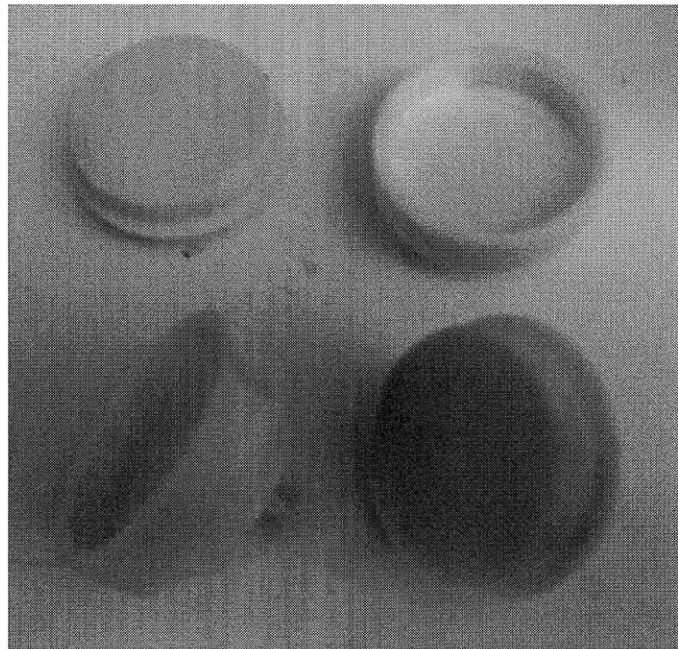


Figure 4-9: Male and female mating parts.

Once the mold for flexible body and the male / female mating parts are ready, next step is to place the mating part and any electronics onto the mold that will go inside the flexible body.

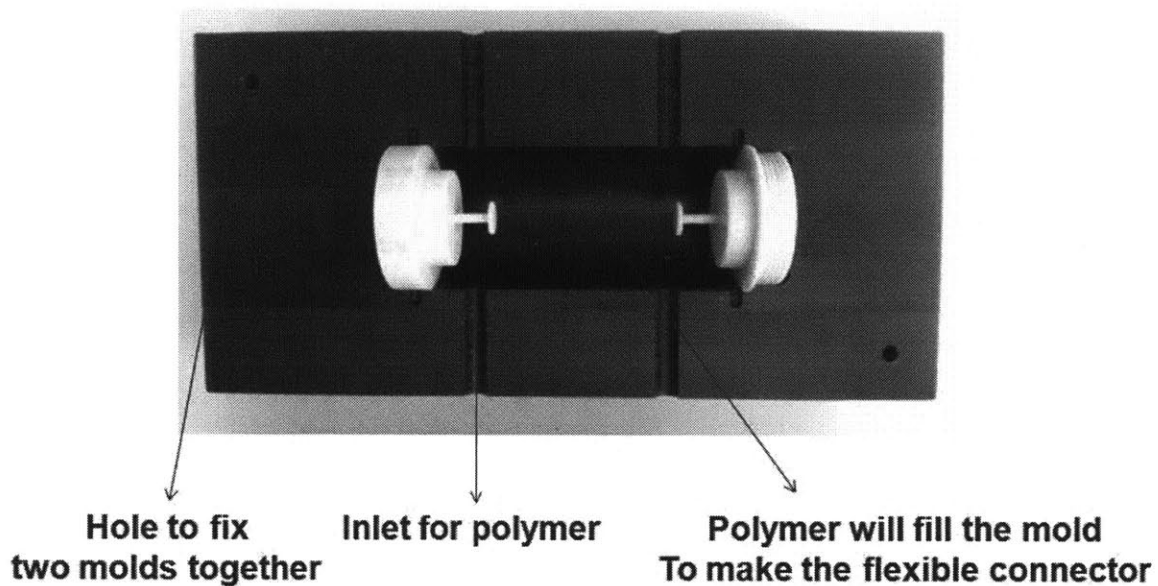


Figure 4-10: Male and female mating parts placed inside the mold.

Figure 4-10 shows the mating parts placed inside the mold. For the prototype purpose, neither electronics nor actuators of any kind have been placed, but it can easily be embedded into the flexible body at this stage. The mold for flexible body has to be two pieces, one for placing the necessary parts to be embedded and the other to close it above. The mold has to have inlet through which soft material will be injected and also it is desirable to have holes where a pin can be placed to fix the mold during the curing process.

After placing all the needed parts, close the mold and firmly fix two molds by

clamps. Then inject the soft material into the mold through the inlet until the mold is completely filled. Several soft materials can be used to make the flexible body. Table 4-1 is from Pablo Valdivia y Alvarado's PhD Thesis [1] that shows material properties of soft materials that can be used. The selection of soft material will largely depend on what kind of flexibility that one wants for the flexible body to have.

Material	Type	$\epsilon$	$E[N/m^2]$	$\mu[Ns/m^2]$
IE10	Polyurethane	0.005	48624	25.8
TD100-11	Polyurethane gel	0.005	4221	0.6
Q300 (1A-1.215B)	Silicone gel	0.02	4373.6	6.4
Q300 (1A-2B)	Silicone gel	0.03	37366.6	52.3
EcoFlex 0010 (no pigment)	Silicone rubber	0.02	97835	92.3
EcoFlex 0010 (orange pigment)	Silicone rubber	0.02	64820	68
EcoFlex 0010 (red pigment)	Silicone rubber	0.02	38417	232
EcoFlex 0010 (green pigment)	Silicone rubber	0.02	56610	82
EcoFlex 0010 (yellow pigment)	Silicone rubber	0.02	95650	90

Table 4-1: Soft materials that can be used for flexible body.

After injecting the soft material into the mold, it requires about 4-6 hours at the room temperature for the curing to complete. The time it takes for the curing process will vary from soft materials used. Once the curing is complete, the rigid-flexible robotic joint can be taken out from the mold.



## 4.5 Prototype

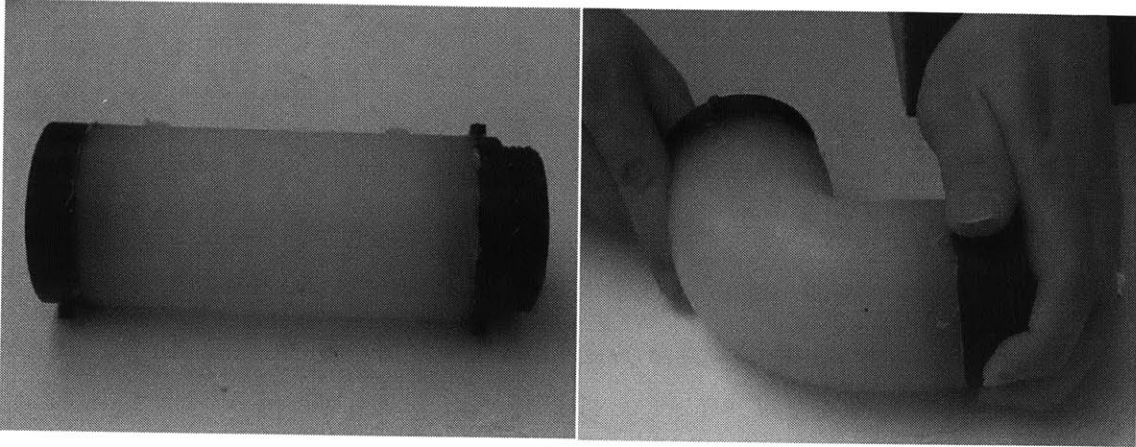
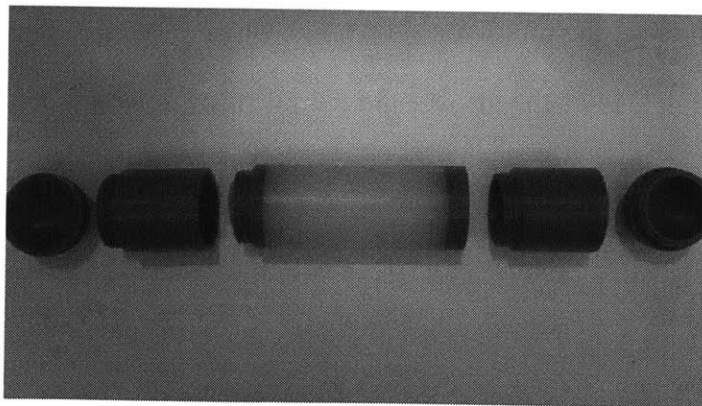


Figure 4-11: First prototype of rigid-flexible joint.

Figure 4-11 shows the first prototype of the rigid-flexible joint built. The material used for the flexible body is silicone rubber. From the figure, one can see that it can easily be bent 90 degrees which will enable it to travel through the t-junctions in the pipe system.

Figure 4-12 shows how the rigid-flexible joint is used to connect the two different rigid modules. The male and female mating part attached at both flexible and rigid module enables the easy connection and disconnection of the rigid modules.



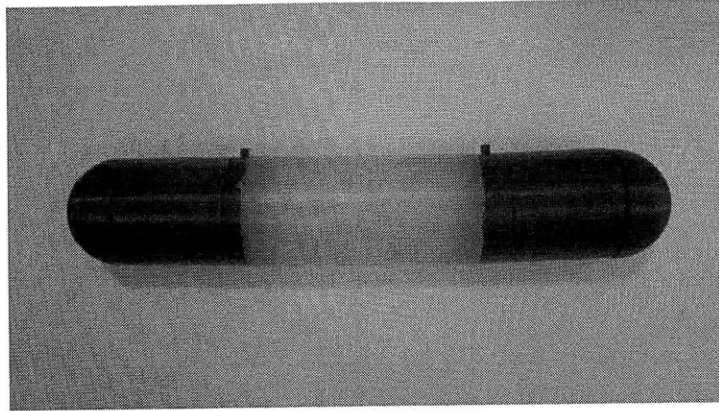


Figure 4-12: Assembly of two rigid modules with rigid-flexible joint.

## 4.6 Experiments

Three experiments are conducted to validate the working of the rigid-flexible joints. They include the ability to negotiate 90 degree t-junction, maintain the shape at pressurized water pipe system and water proof for parts embedded inside.

### 4.6.1 Test for Bends

The rigid-flexible joint is tested for the ability to travel through the bends in the water pipe system. For the test, the prototype shown in figure 4-12 was used. The length of the prototype is such that if it was made of rigid module only, it would certainly get stuck in the 90 degree bends. The prototype was placed inside the water-pipe experiment setup used for sensor testing and was passively moved by the water flow.

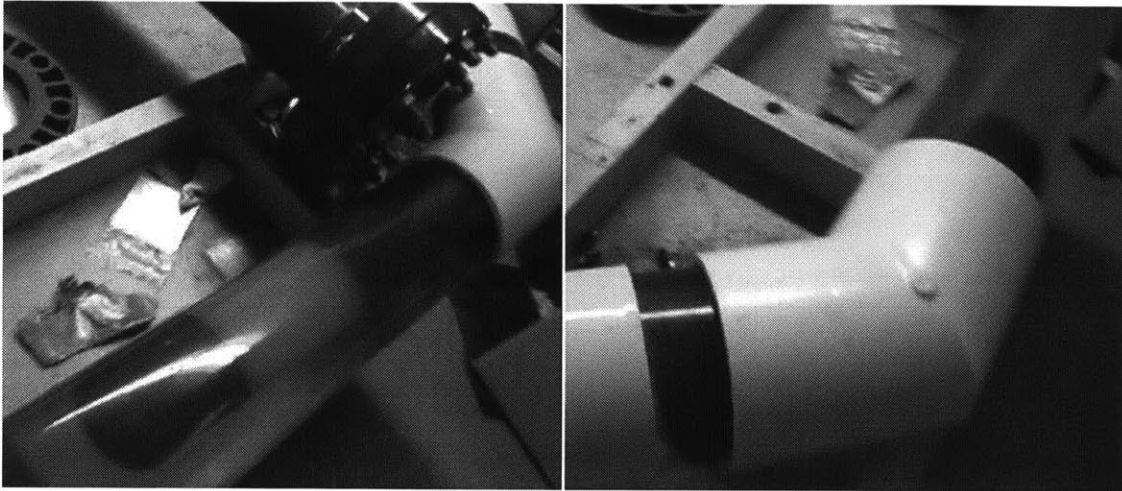


Figure 4-13: Rigid-flexible joint prototype traveling through the bends.

Figure 4-13 shows the photo of prototype taken while the placed inside the pipe. Though the vision of action through the junctions is impaired by the opaque pipe parts, one can clear see how the two dummy rigid modules connected by rigid-flexible joint can travel through the bends despite being not short in length.

#### **4.6.2 Test for Pressure**

Since the rigid-flexible joint is to be used under the pressurized water pipe system, a test is performed to see if it can maintain the shape under pressurized water. The ability to maintain the shape is important because if the shape was to change under pressure, it might result in increase of drag coefficient by deviating from the desired shape. Several shapes were tested under different pressure and the result showed that the shapes remain intact even at 54psi which is the maximum pressure of water pipe system. Figure 4-14 shows photos taken for one of the shapes that were tested.

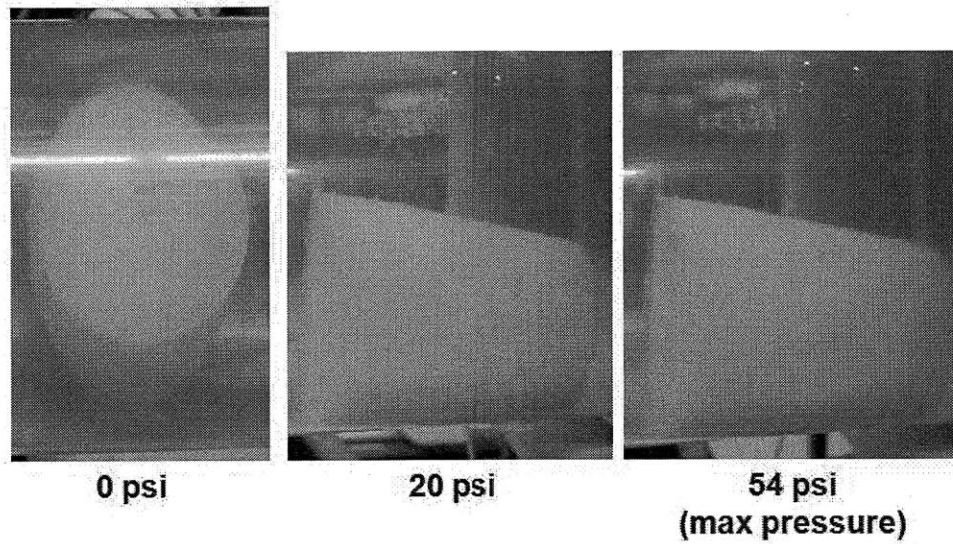


Figure 4-14: Pressure test for the cylindrical shape with hollow inside.

### 4.6.3 Test for Water-Proof

The rigid-flexible joints need to be water proof for any embedded electronics to safely work. To test for the water-proof, a dry cotton wool was placed inside a cavity of a cylindrical flexible body as shown in Figure 4-15.

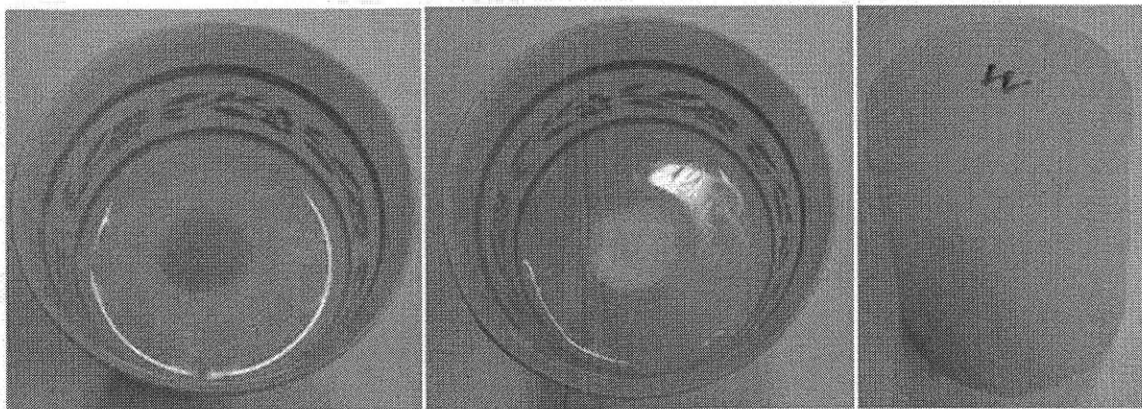


Figure 4-15: Cylindrical flexible body with cotton wool filled inside.

The flexible body with dried cotton wool was weighed and then placed inside water pipe system with maximum pressure of 54psi. After 30 minutes of immersion, it was taken out and weight was taken again. The result showed no change in the weight before and after the immersion. This indicates that the dried cotton wool inside was protected from water outside validating the flexible body's ability for water-proof.

## **4.7 Conclusion**

This chapter dealt with the concept of rigid-flexible joints, the design and manufacturing process and presented prototypes built and some of experiments performed. The resulting prototype showed promise of rigid-flexible joint that could enable the robotic platform to travel through the bends. In addition, it provides continuous overall shape that greatly reduces the drag coefficients and housing for electronics to be embedded. Although the prototype showed in this chapter did not include embedded actuators or electronics, it is certainly possible to incorporate these components inside the rigid-flexible joints. A further work in has been done but will not be discussed in this thesis.



# **Chapter 5**

## **Friction Controlling Mechanism**

### **Using Magnetic Force**

#### **5.1 Abstract**

In this chapter, novel mechanism that generates controllable friction for in-pipe robot with minimal energy is presented. Detail of how permanent magnet is used in the mechanism to achieve the objective is discussed as well as important design parameters identified. Analysis of the mechanism is performed with appropriate modeling of the magnet and the relation between the design parameters and the performance is shown. Also built prototype of the mechanism is presented as a proof of concept.

#### **5.2 Introduction**

Pipe system is perhaps one of the most important infrastructure in the modern society that

effectively transports valuable resources such as oil, gas and water. Therefore, continuous and careful monitoring and inspection of the pipelines are needed to ensure the proper working of the system. However, most of the pipelines are buried under the ground that is beyond reach of human operators. Hence, a large number of in-pipe robots are developed with the purpose of carrying out an inspection inside the pipelines of interest.

Among different locomotion strategies employed by in-pipe robots, using wheels attached on leg is most common as wheels provide efficient means of propulsion [1]. These wheeled in-pipe robots require certain ways of providing pressing force on the wheels to maintain the traction. Some of these in-pipe robots passively exert this normal force on the wheel by having leg with pre-designed stiffness [2]. On the other hand, several in-pipe robots have active normal force generating mechanism that can create varying friction [3-10].

Being able to control the normal force applied on the wheel is desirable for number of reasons. First, friction force to maintain traction may vary for different situations. For example, in-pipe robot traveling through vertical section of the pipe will definitely need more friction force than when moving horizontally. Passive normal force applying mechanism can only provide pre-defined amount of friction and thus may fail to keep traction certain situations. Also, with appropriate feedback control, active mechanism can provide just enough friction force to keep traction and not apply unnecessary excess friction. This can greatly reduce the torque requirement of the motor driving the wheels.



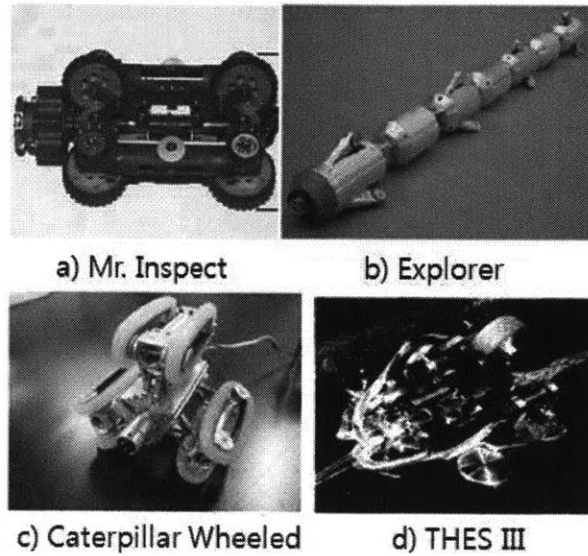


Figure 5-1: Examples of wheeled in-pipe robots with active friction varying mechanism.

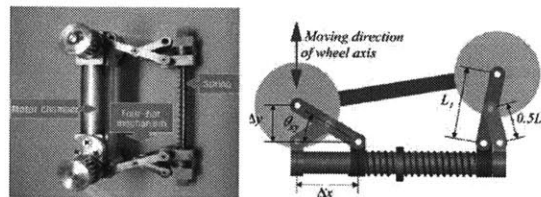


Figure 5-2: Typical three bar linkage mechanism used to provide active friction force.

Fig. 5-1 shows some of the in-pipe robots that have active normal force generating mechanism to vary the friction applied on the wheel. All these in-pipe robots typically use three bar linkage with compliant link to actively provide the friction force as shown in Fig. 5-2 and has advantage over the passive counterparts. However, the three bar linkage mechanism commonly used by in-pipe robots have shortcoming of being energy inefficient. That is higher the friction force need to be generated, higher the torque

required of the motor activating and controlling the three bar linkage which in turn leads to great energy consumption.

In this chapter, a novel mechanism capable of generating large range of controllable friction with very low torque requirement is presented. Low torque requirement ensures that only minimal energy is consumed in providing the controlled friction which can greatly lengthen the operation time of the in-pipe robots.

### 5.3 Overview of Mechanism

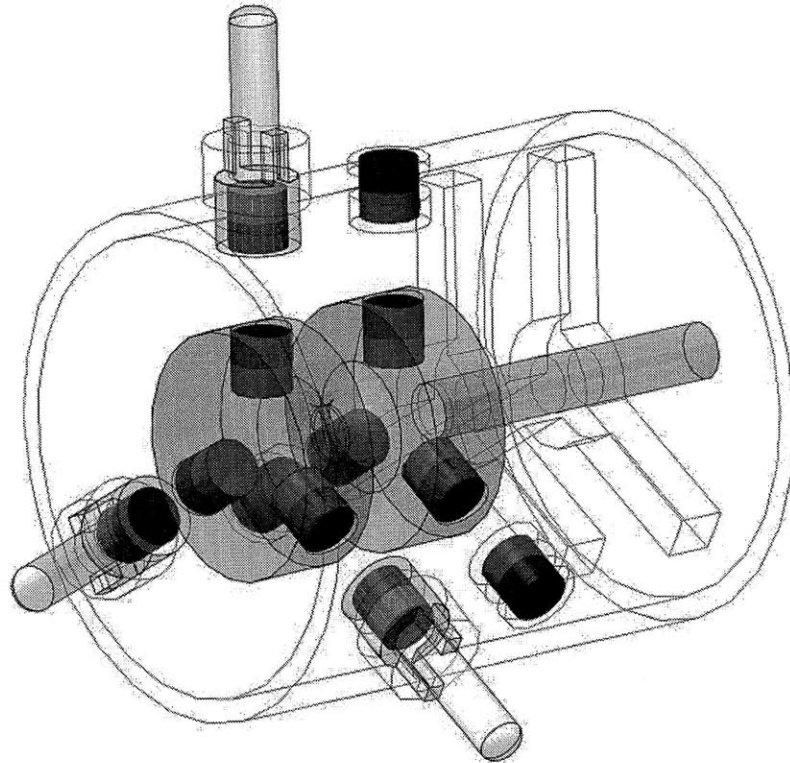


Figure 5-3: Overview of the mechanism.

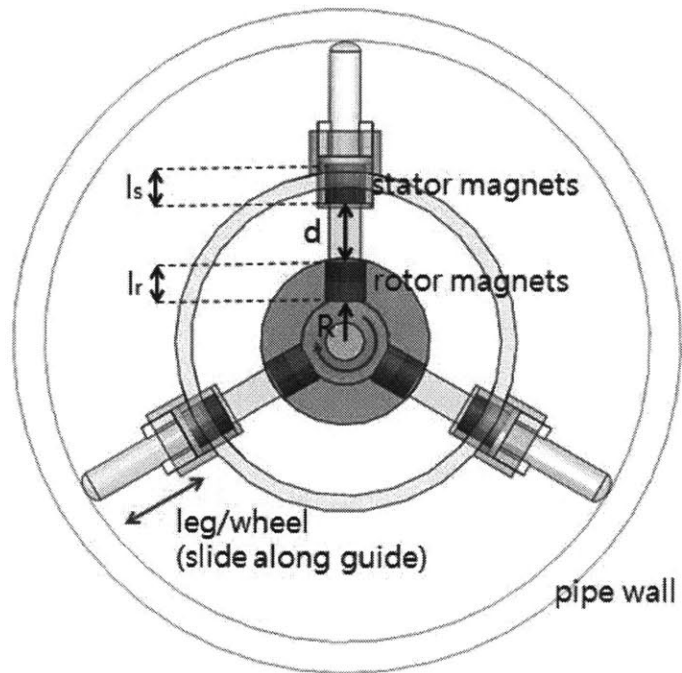


Figure 5-4: Front view of the mechanism.

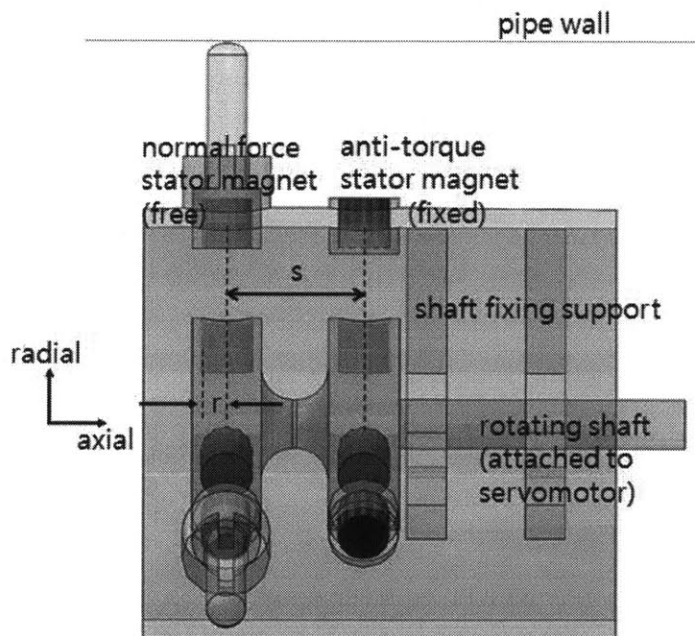


Figure 5-5: Side view of the mechanism.

### 5.3.1 Description

The mechanism described in this chapter makes use of a magnetic force between permanent magnets to produce controlled normal force on the wheel/leg of the in-pipe robot. Fig. 5-3 gives the overview of the mechanism with Fig. 5-4 and Fig. 5-5 showing front and side view. The mechanism consists of a set of stator magnets that are placed on the circumference of the in-pipe robot and a set of rotor magnets attached to a disk rotated by a shaft connected to a servomotor.

The set of stator magnets consist of two pairs. One pair of stator magnet is attached to the end of each leg/wheel with north pole facing inward. This pair of stator magnets can move freely in the radial direction as the leg/wheel slides along the guide. The other pair of stator magnet is placed along the circumference of the in-pipe robot at certain distance away in the axial direction from the first pair. This second pair of stator magnets is fixed and most importantly has magnetic poles reversed from the first pair with north pole facing outward.

The set of rotor magnets also consist of two pairs. Each pair is mounted on a disk with both pair having north pole facing outwards. Two disks with rotor magnets are attached to a single shaft which rotates in the axial direction. The distance between the two disks and their respective position along the axial direction is such that set of stator magnets are directly above the rotor magnets. (It is noted that both stator and rotor magnets are symmetrically placed with equal spacing.)

### 5.3.2 Design Parameters

Fig. 5-4 and Fig. 5-5 shows some of the design parameter involved with the mechanism. The important design parameters that affect the performance of the mechanism are listed as follow.

$r$  = radius of rotor/stator magnets

$l_s$  = length of the stator magnet

$l_r$  = length of the rotor magnet

$R$  = distance from disk center to south pole of rotor magnet

$d$  = distance between rotor and stator magnet when aligned coaxially

$s$  = separation distance between two pairs of stator/rotor magnets

$N_s$  = number of stator magnets in one pair

$N_r$  = number of the rotor magnets in one pair

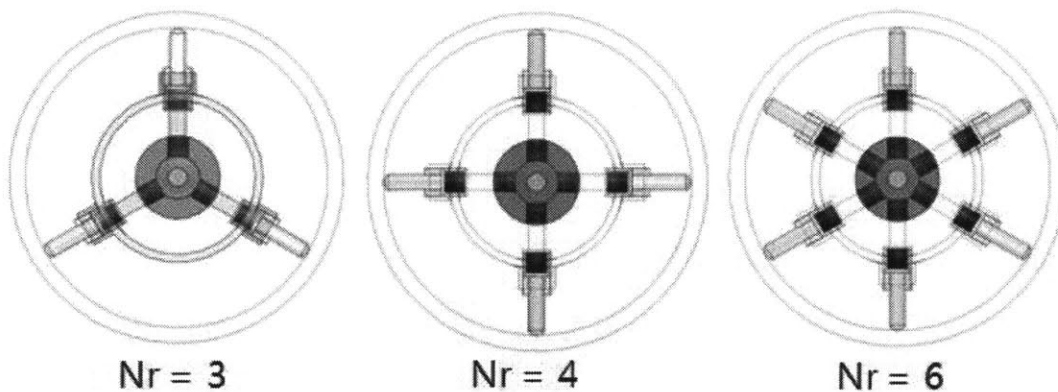


Figure 5-6: Mechanism with different number of rotor magnets.

Fig. 5-6 shows mechanism with different number of rotor magnets with  $N_s = 3, 4, 5$ . The number of rotor magnets corresponds to the number of leg/wheel that the in-pipe robot has. The mechanisms shown in the figure also has same number of stator magnets as rotor magnets with  $N_r = 3, 4, 5$ . Since each leg/wheel has one stator magnet attached, the number of stator magnets has to be equal to and cannot be smaller than the number of rotor magnets. However, number of stator magnets can be greater than the number of rotor magnets.

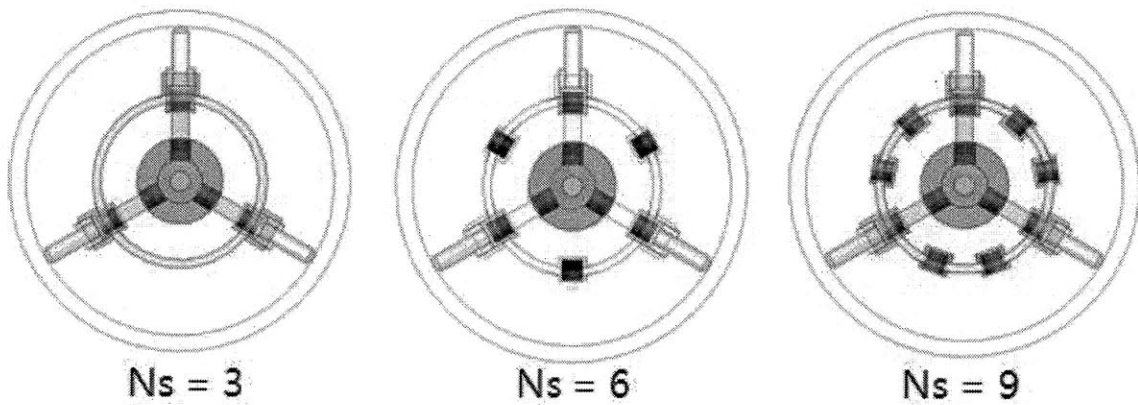


Figure 5-7: Mechanism with different number of stator magnets.

Three mechanisms shown in Fig. 5-7 all have  $N_r = 3$ . Nevertheless, the number of stator magnets varies with  $N_s = 3, 6, 9$ . Here, the stator magnets that are not attached to the leg/wheel are fixed on the circumference of the in-pipe robot and thus cannot be moved. Also, number of stator magnets cannot be arbitrary number but only multiple of number of rotor magnets. That is  $N_s = k N_r, k \in \mathbb{Z}^+$ .

All the design parameters listed here have significant effect on the performance of the mechanism, especially on the shape of normal force and torque curve produced. Their exact effect will be discussed in more detail Section III.

### 5.3.3 Generating a Controllable Normal Force

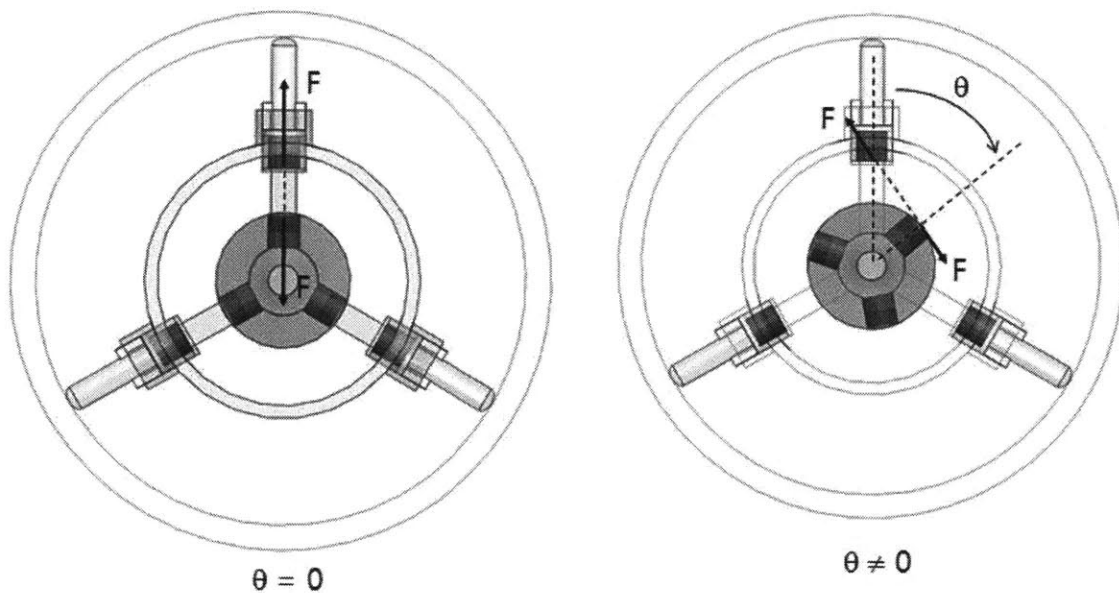


Figure 5-8: Configuration of stator/rotor magnet with angle  $\theta$ .

The front pair rotor and stator magnet works to produce the controllable normal force. The magnetic force on the stator magnet attached to the leg/wheel by the rotor magnet produces the normal force on pipe wall which in turn creates friction. Here, a new variable  $\theta$  is introduced which equals the angle between two axis of rotor and stator magnet. This angle  $\theta$  is not a design parameter, but a variable that is controlled by the

rotating angle of shaft via servomotor.

Fig. 5-8 shows two instances where  $\theta = 0$  and  $\theta \neq 0$  with repulsion force between north poles of rotor/stator magnets indicated. Qualitatively speaking, the repulsion force decreases as the distance between the north poles increases. When  $\theta = 0$ , the distance between the north poles is closest and the repulsion force is in the direction of the normal force. Thus, it is clear that maximum normal force is produced at this instance. As the shaft rotates, the relative position of rotor magnet with respect to stator magnet changes. As  $\theta$  increases, the distance between the north poles also increases and the direction of repulsion force deviates more from the direction of the normal force. From this fact, it can be inferred that normal force produced by the mechanism will decrease as  $\theta$  increases, meaning normal force produced is a function of angle  $\theta$ . Therefore, by obtaining an accurate  $F_n$ - $\theta$  curve and controlling the angle  $\theta$ , the normal force  $F_n$  generated by the mechanism can be controlled.

However, for every action there is a reaction. Magnetic force on stator magnet by rotor magnet produces desirable normal force, but equal and opposite magnetic force on rotor magnet by stator magnet produces torque on the shaft that needs to be overcome by servomotor. The greater the desired normal force, the greater the required torque. Since torque integrated over the angle  $\theta$  gives energy, high torque directly relates to high energy consumption. Thus, a front pair of stator/rotor magnet alone cannot produce normal force in an energy-efficient way.



### 5.3.4 Cancellation and Reduction of Torque

For the mechanism to generate normal force with minimal energy consumption, the torque imposed on the shaft must be reduced. The rear pair of rotor and stator magnet is incorporated into the mechanism for this purpose.

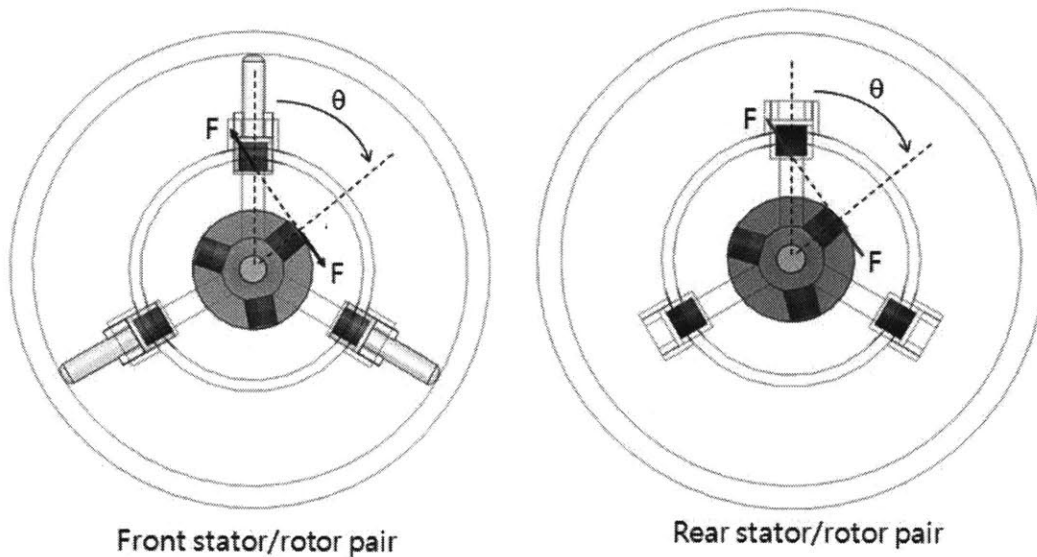


Figure 5-9: Comparison of magnetic forces in front and rear stator/rotor pair.

Fig. 5-9 shows a magnetic force between front and rear pair of stator/rotor magnet at given angle  $\theta$ . Configuration wise, both front and rear pair of magnets are in the same location. Nevertheless, there are two main difference between the two pairs.

First, the stator magnet on the front pair is attached to end of the leg/wheel whereas the stator magnet on the rear pair is fixed on the circumference of the in-pipe robot. Therefore, the magnetic force on stator magnet by rotor magnet in the rear pair does not contribute to the normal force generated on the pipe wall.

Second, the poles of the stator magnet on the rear pair is opposite of that of front pair. This means the force acting on the rotor magnet by stator magnet in the rear pair is equal but opposite in direction from that of front pair. Thus, the torque produced by the front stator/rotor magnet pair on the shaft is exactly cancelled out by the torque that rear pair produces.

Theoretically speaking, the shaft in the mechanism should experience zero torque for any angle  $\theta$  due to cancellation of torque due to symmetry. However, because the magnetic force is highly sensitive to the distance and hence machining error causing misalignment of front and rear pair magnets, it is desirable to reduce the magnitude of the torque itself produced by the front pair of stator/rotor magnet. This can be achieved by increasing the number of stator magnets as shown in Fig 5. It is similar to conventional way of reducing the motor cogging torque by increasing the number of poles. The exact effect of increasing number of stator magnet has on torque reduction will be discussed more in Section III.

Also, if stator magnet of the rear pair is too close to the stator magnet of the front pair, it will affect the normal force produced to some degree. This effect can be almost neglected when the separation distance between front and rear pair is twice the diameter of the magnet. Hence, it is desirable to have  $s \geq 4R$ .

## 5.4 Analysis of Forces and Effects of Design Parameters

### 5.4.1 Methods of Calculating Magnetic Force

The desired normal force range for a specific application requires appropriate values for the design parameters. Therefore, a quantitative analysis is necessary for relating the design parameters to the torque and the normal forces acting on each leg.

The most commonly used method in calculating the magnetic forces between magnets is the use of magnetic circuit concept. However, this method requires the system to have dominant magnetic pathline and negligible air gap effects. Since the mechanism does not have dominant magnetic pathline with high permeability and has significant air gap between the magnets, it is not valid for this purpose.

In the literature, a number of papers describe analytical method of calculating of magnetic force between magnets with parallel axis. D. Vokoun et al. [1] uses Maxwell equation and magnetostatic interaction to derive the analytical expression for force between two cylindrical magnets with common axis (assumes uniform magnetization). When adopted using design parameters, it is written as follows where M is the magnetization

$$F = 4\pi\mu_0 M^2 r^2 \int_0^\infty \frac{J_1^2(q)}{q} \sinh\left(\frac{ql_c}{2r}\right) \sinh\left(\frac{ql_r}{2r}\right) e^{-q\left(\frac{l_c+l_r}{2}\right)} dq \quad (5.1)$$

This formula gives accurate value for the magnetic force between the stator and rotor magnets when  $\theta = 0$  and is verified through experiments. Thus, it can be effectively

used to calculate the maximum normal force produced for a given design parameter values. J. S. Agashe et al. [2] uses Kelvin formula to derive similar expression that gives the magnetic force between cylindrical magnets having a common axis. Other papers also discuss magnetic force between magnets of different shapes (e.g. cubic) but having parallel axis.

These analytical approaches, though precise, are not useful for two reasons. First, analytically derived expressions for magnetic force involve complex terms that make it difficult to understand the effect of changes in the value of the design parameters. Second, more importantly, they all describe magnetic forces between magnets having parallel axis and thus cannot be used to calculate magnetic forces between stator/rotor magnets when  $\theta \neq 0$  needed in our case.

There exists a number of FEM software (e.g. Maxwell) that can be used to calculate the forces between the magnets of arbitrary configuration. Nevertheless, using FEM software does not give any insight into the effects design parameters have on the forces created so it can only be used as a verification tool not a designing tool.

Considering such limitations in the different methods of calculating magnetic force described above, use of magnetic dipole where the magnet is modeled as two magnetic charge of equal magnitude and opposite sign is used for the analysis. This method provides the following advantages – ability to calculate magnetic force between the magnets in arbitrary configuration, easiness of calculation, and importantly, the effect of design parameters become explicit.

### 5.4.2 Modeling of Magnet

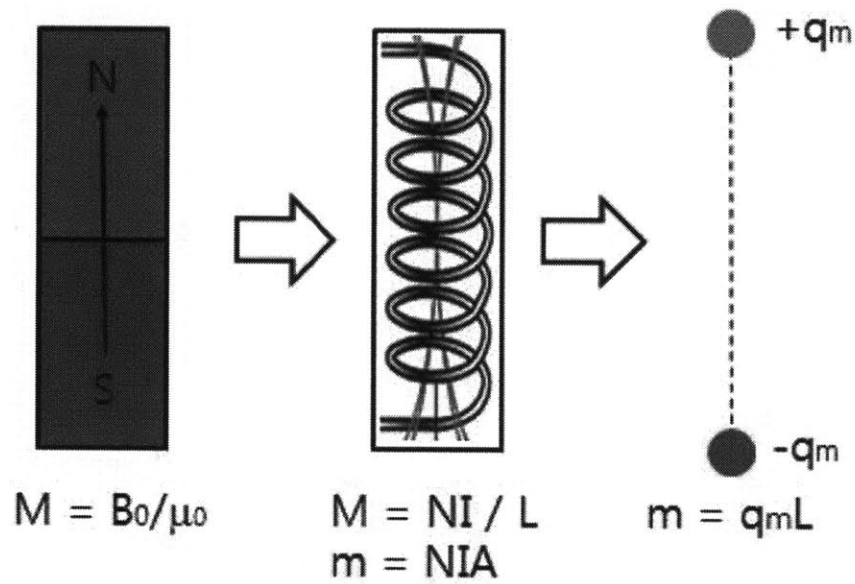


Figure 5-10: Steps in modeling a magnet as equivalent magnetic charge.

Fig. 5-10 shows the steps in modeling of a magnet. First, magnet is modeled as a solenoid of  $N$  turns with current  $I$  having area  $A$  and length  $L$  same as the original magnet. Then this solenoid is transformed into two magnetic charges  $+q_m$  and  $-q_m$ . The value of magnetic charge  $q_m$  can be found as follow.

Assuming a uniform magnetization ( $M$ ) in the magnet and since there is no external magnetizing force ( $H=0$ ),  $M$  can be written as

$$M = B_0 / \mu_0 \quad \square \quad H = B_0 / \mu_0 \tag{5.2}$$

For solenoid, the magnetization is given by

$$M = NI / L \quad (5.3)$$

Equating Equations (5.2) and (5.3) leads to,

$$NI = B_0 L / \mu_0 \quad (5.4)$$

The magnetic moment ( $m$ ) of the solenoid is given by

$$m = NIA \quad (5.5)$$

And the magnetic moment of magnetic charge is

$$m = q_m L \quad (5.6)$$

Combining Equations (5.5) and (5.6),  $q_m$  is expressed as

$$q_m = NIA / L \quad (5.7)$$

Substituting Equation (5.4) into (5.7) and using  $A = \pi r^2$ ,  $q_m$  becomes

$$q_m = B_0 \pi r^2 / \mu_0 \quad (5.8)$$

Where  $\mu_0$  is the permeability of free space and  $B_0$  can be found from remanance of a magnet used.

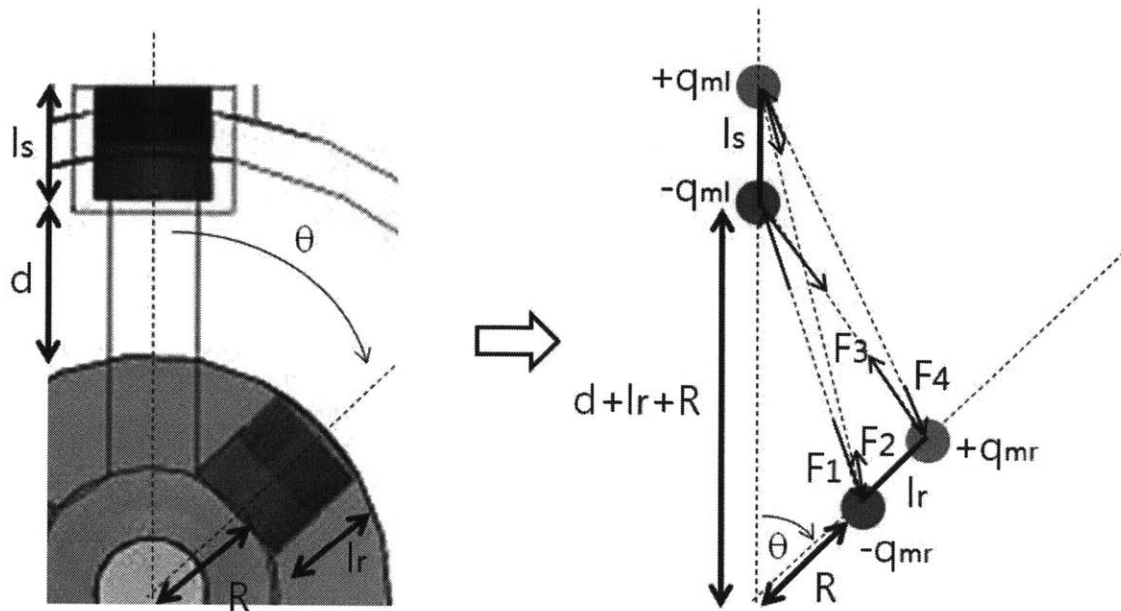


Figure 5-11: Magnetic forces acting on typical stator/rotor configuration.

Now using the equivalent magnetic charge of the magnet derived from above, magnetic force between two magnets in arbitrary position can be calculated. Fig. 5-11 shows typical configuration of stator/rotor magnet with angle  $\theta$ . The magnetic force between two magnetic charges act along the line connecting the two and is given by

$$F = \frac{\mu_0}{4\pi} \frac{q_{mr}q_{ml}}{x^2} \quad (5.9)$$

Where  $x$  is the distance between the two charges. Four pairs of magnetic forces, two repulsive and two attractive, act on stator/magnet and from these forces, normal force and torque generated by the mechanism can be calculated. This model gives accurate value from the region where two magnets are separated by distance equal to its radius. If the two magnets are close, the value start to deviate from the analytical solution.

### 5.4.3 Forces and Torques for Single Stator/Rotor Magnet

To see the effects that design parameters have on the normal force generated and torque, let us first look at the forces and torques of single stator/rotor magnets.

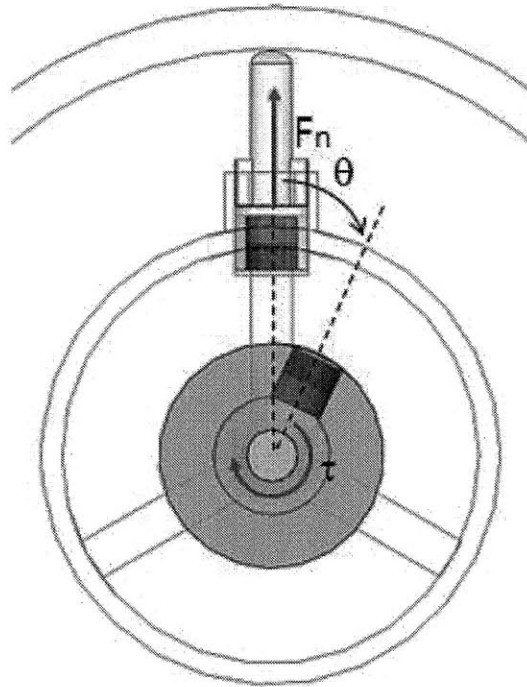


Figure 5-12: Forces and torques on single stator/rotor magnet.

At angle  $\theta = 0$ , the normal force  $F_n$  is maximum with  $\tau = 0$ . At this instance, the normal force  $F_n$  can be calculated using equivalent magnetic charges. Taking the length of the stator magnet same as the length of rotor magnet ( $l_s = l_r = l$ ), maximum normal force given by expression



$$F_n \Big|_{\max} = \frac{\pi B_0^2 r^4 l^2}{\mu_0 d^2 (d \oplus 2l)^2} \quad (5.10)$$

Equation (5.10) gives scaling laws of design parameters that could be used in the desired normal force tuning.

The radius of the magnet has most dominant effect on the maximum normal force produced.  $F_n$  is proportional to radius to power 4, meaning a small change in the magnet radius could greatly increase or decrease the normal force.

The distance between the magnets also has a significant effect. When the distance between two magnets are equal or smaller than the length of the magnet ( $d \leq l$ ), the normal force increases inversely proportional to the distance power 2. Nevertheless, as distance between two magnets become significantly greater than the length of the magnet ( $d \gg l$ ), the normal force falls to the power 4 of increase in the distance.

The length of the magnet is least effective in changing the normal force. Decreasing the length of magnet below the distance between the magnets will significantly reduce the normal force by a power 2, but increasing the length above the separation distance will not bring about much change. The strength of the magnet (remanence) used is also related to  $F_n$  by the power of 2. These scaling laws relating the design parameters to the normal force give a useful guide in selecting the value of design parameters.

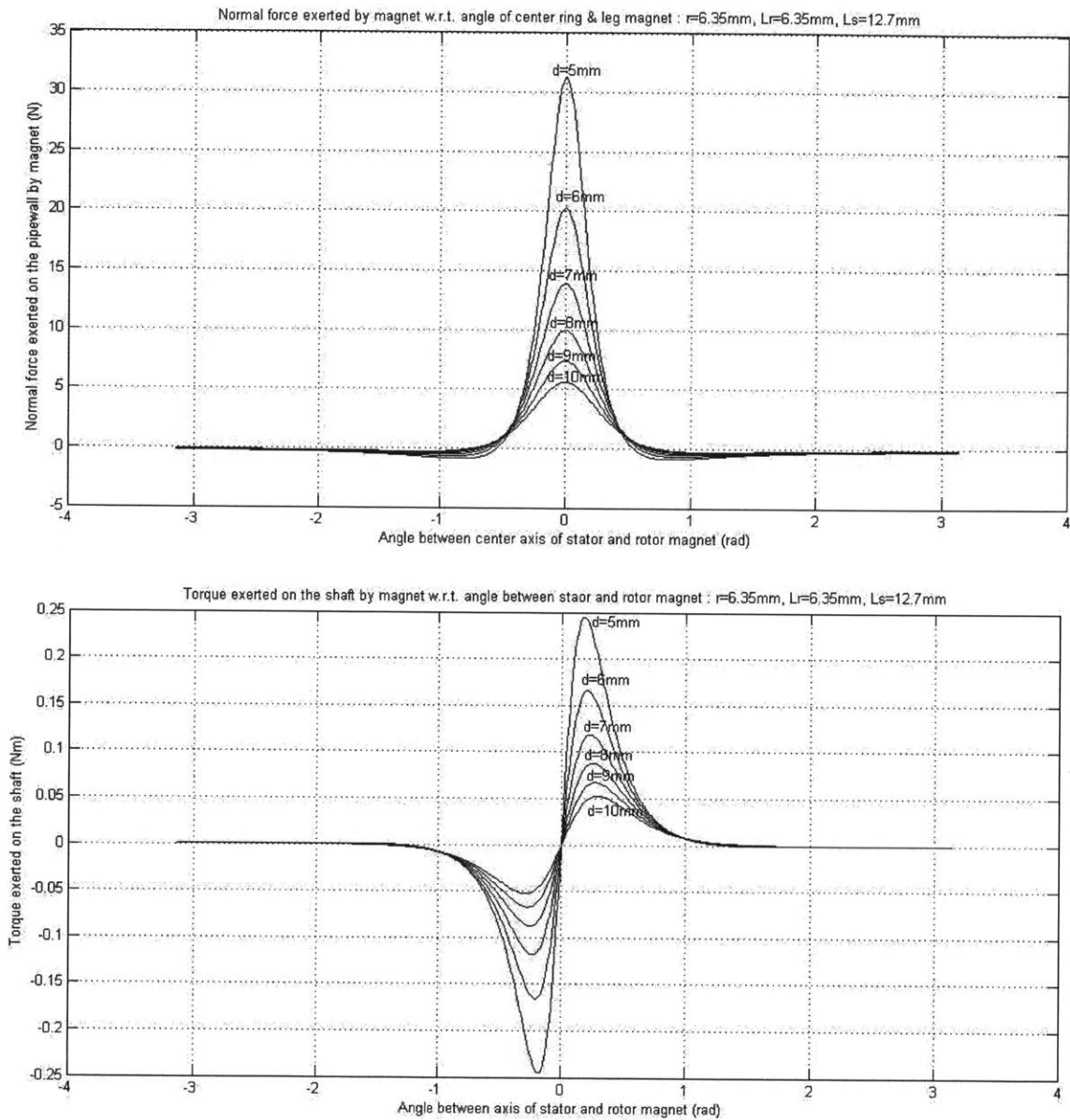


Figure 5-13: Normal force and torque produced with single stator/rotor magnet.

Fig. 5-13 shows how the normal force on the pipewall and torque on the shaft changes as the angle  $\theta$  goes from  $-\pi$  to  $+\pi$  for different value of  $d$ . As expected, the maximum normal force occurs when  $\theta = 0$ . But what is more interesting is that the

normal force actually becomes negative value around  $40^\circ - 60^\circ$  with exact value depending on the distance  $d$ . Where the normal force switches from positive to negative is the point where repulsion force from like poles are exactly cancelled out by attraction of opposite poles. This phenomenon is desirable because it means that the servomotor controlling the shaft rotation only needs to turn from  $0^\circ$  to around  $50^\circ$  to provide a normal force from zero to  $F_n$  maximum.

The torque graph indicate that although  $\tau = 0$  when  $\theta = 0$ , this is an unstable equilibrium point. The torque sharply increase with small deviation from  $\theta = 0$  and reaches maximum between  $10^\circ$  and  $20^\circ$ . Also note that, a smaller distance between stator/rotor magnets that produces large normal force, also creates high torque.

#### **5.4.4 Forces and Torques for Multiple Stator/Rotor Magnets**

Fig. 5-6 shows mechanism with different number of rotor magnets with equal number of stator magnets. Fig. 5-14 and Fig. 5-15 show graphs of the simulated normal forces and torques for two cases, namely when  $N_r=N_s=3$  and  $N_r=N_s=6$ .

The number of rotor magnets ( $N_r$ ) corresponds to the number of leg/wheel. Therefore it is expected that the magnitude of the normal force and torque will increase as  $N_r$  increases and it can be easily seen from the graphs in Fig. 5-14 and Fig. 5-15.

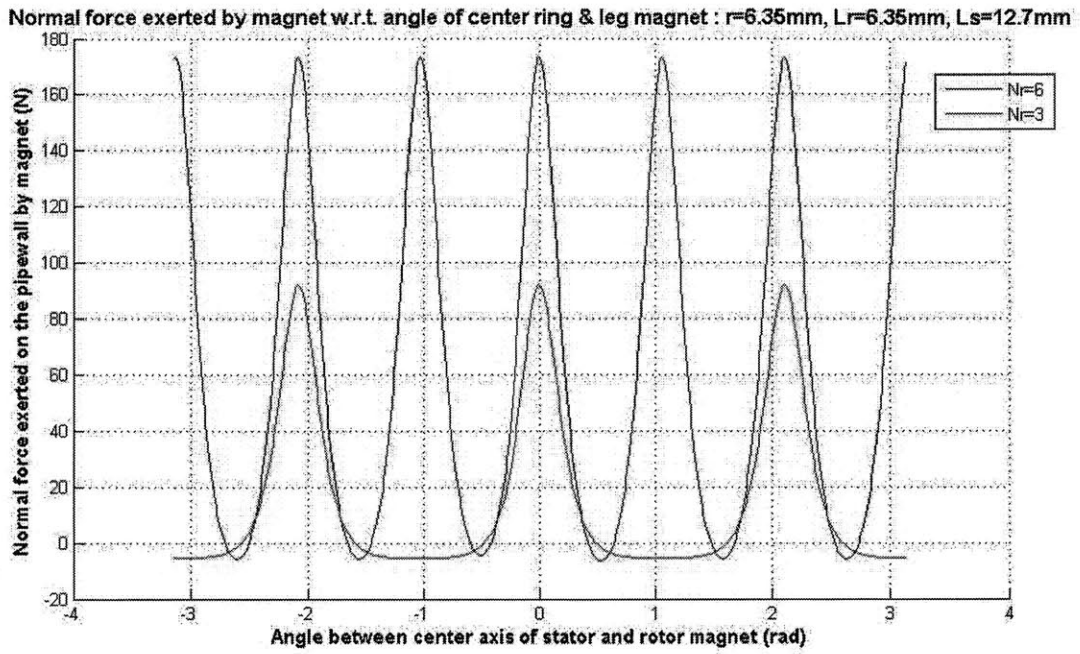


Figure 5-14: Comparison of normal force produced for  $N_r=N_s=3$  and 6.

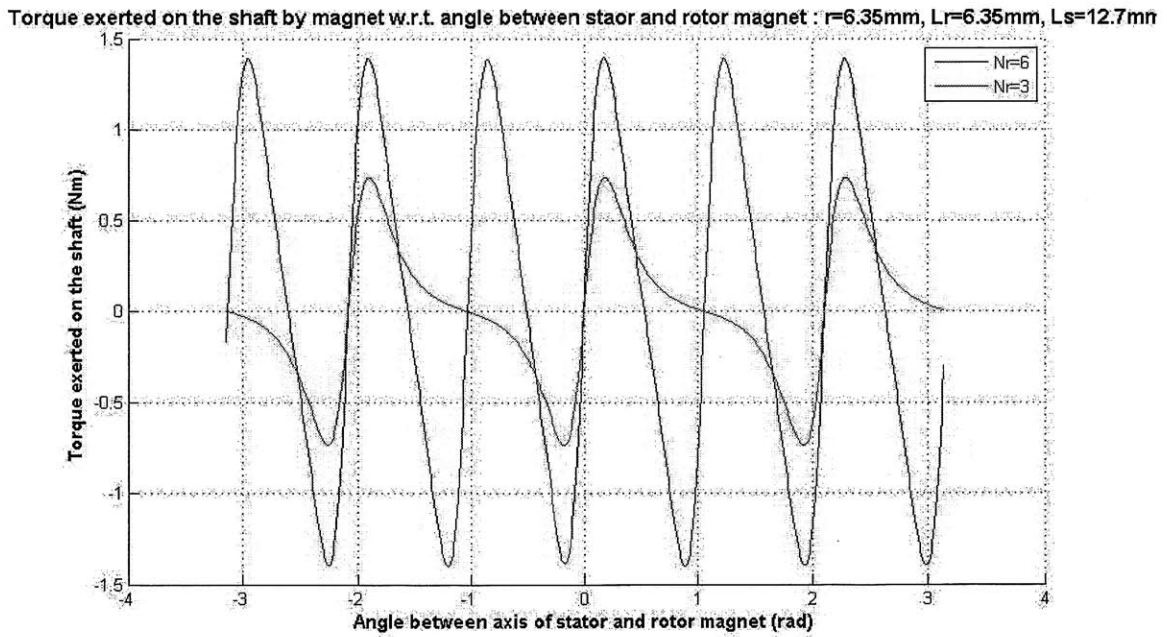


Figure 5-15: Comparison of torque produced for  $N_r=N_s=3$  and 6.

For the normal force produced, it is interesting to note that as  $N_r$  increases, the point where the normal force changes sign decreases. Narrowing of the peak width coupled with increase in normal force results in a steep gradient in the  $F_n-\theta$  curve. This makes  $F_n$  highly sensitive to change in angle. This allows the production of large range in the normal force with small operating angle range. Nevertheless, it also deteriorates the resolution of the normal force produced so there is a tradeoff.

For the torque exerted on the shaft, it is zero at every configuration where the rotor magnet is between the stator magnet. This point is a stable equilibrium point and the shaft will resist any torque driving it away from it. The shaft moves away from this position when sufficiently high external torque is applied that exceeds maximum torque shown on the graph. This corresponds exactly to the cogging torque experienced by conventional motors.

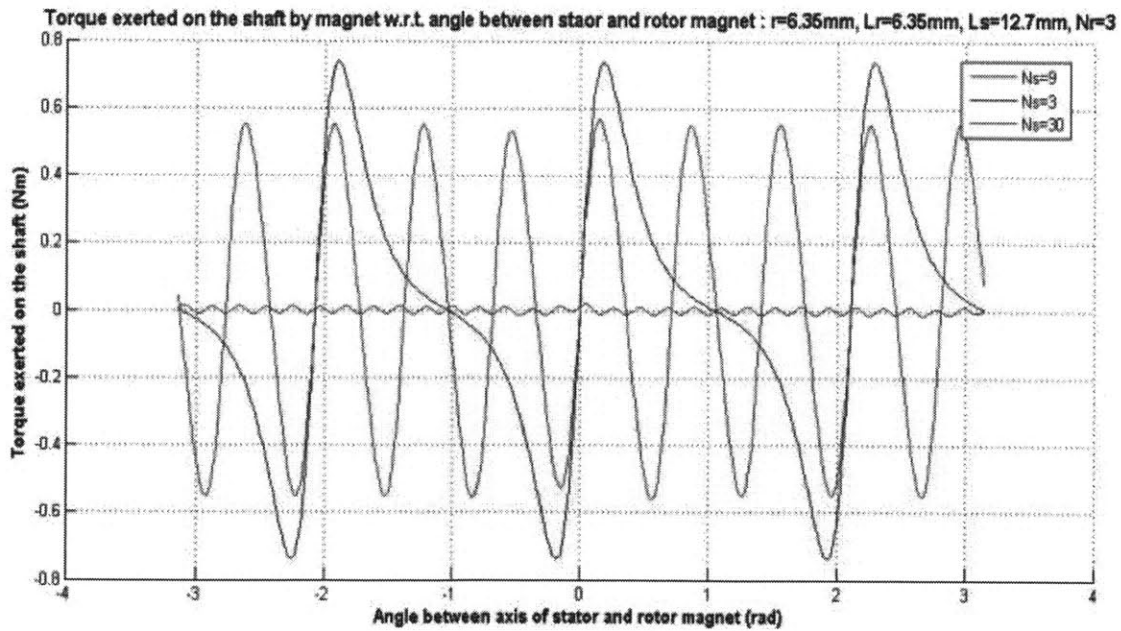


Figure 5-16: Effect of increasing stator magnets on torque.

While increasing the number of rotor magnets ( $N_r$ ) augments both the normal force and torque, increasing only the number of stator magnet ( $N_s$ ) while keeping  $N_r = \text{const.}$  can significantly reduce the torque exerted on the shaft while maintaining a normal force produced. Fig. 5-16 shows  $\tau-\theta$  graph varying  $N_s = 3, 9, 30$  with  $N_r=3$  for all three. The result shows significant drop in the torque whereas the normal force, though not shown here, remains almost the same. However, if the value of  $N_s$  become too high, the fixed stator magnet next to free stator magnet attached to the end of leg/wheel becomes close enough to alter the normal force produced and may have undesirable effect on controlling the normal force.

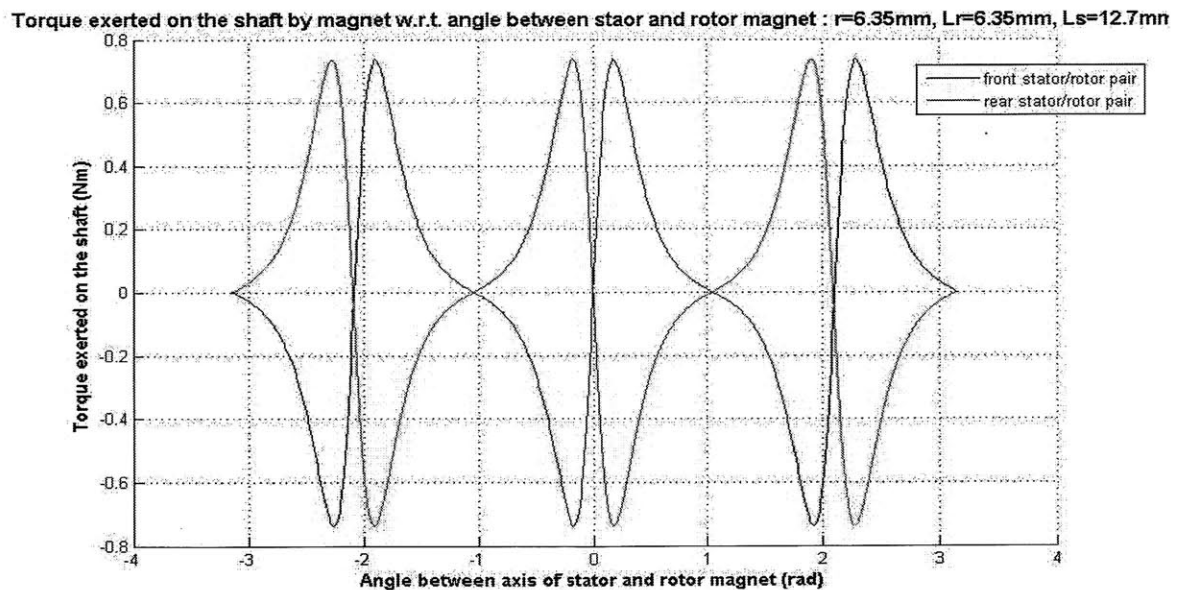


Figure 5-17: Torque cancellation effect of rear pair of stator/rotor magnet set.

The rear pair of the stator/rotor magnet discussed in the Chapter 5.3 provides a

more effective way of reducing the torque on the shaft. The front and the rear pair of stator/rotor magnet being in the same configuration but having opposite polarity results in two pairs producing equal but opposite torque as shown in Fig. 5-16. This not only reduces but nearly cancels out the torque enabling generation of large normal force with minimal energy consumption.

## 5.5 Prototype as Proof of Concept

Two prototypes were built to prove the feasibility of the mechanism discussed and verify the theoretical analysis of the mechanism. Parts were manufactured using a 3d-printer with ABS plastic as the raw material and NeFdB magnets were used for both the stator and rotor magnets.

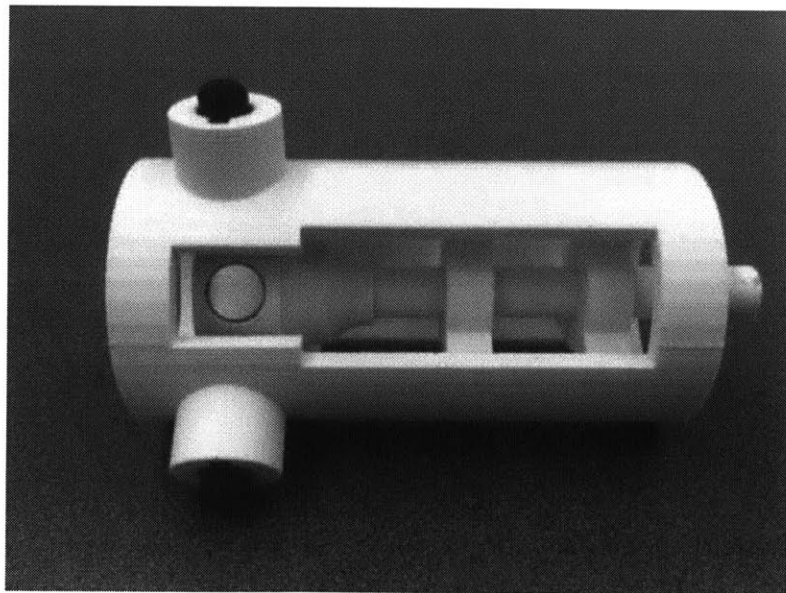


Figure 5-18: Prototype I with only front stator/rotor pair.

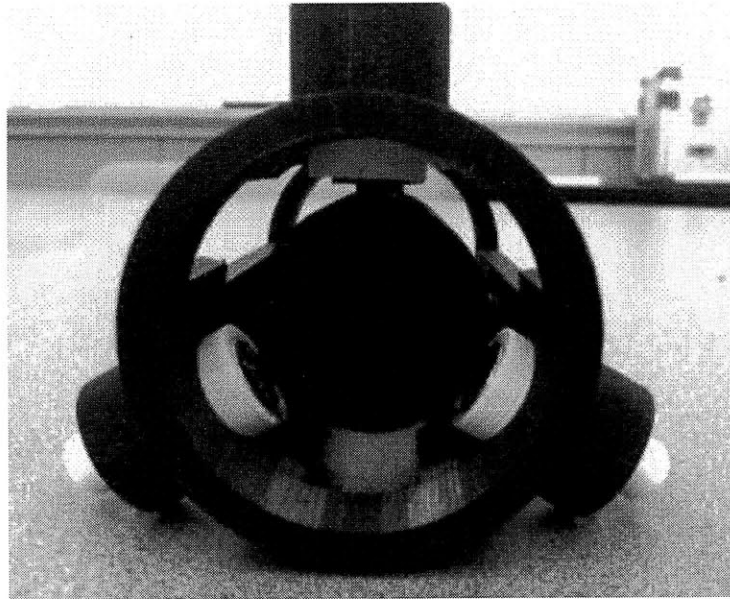
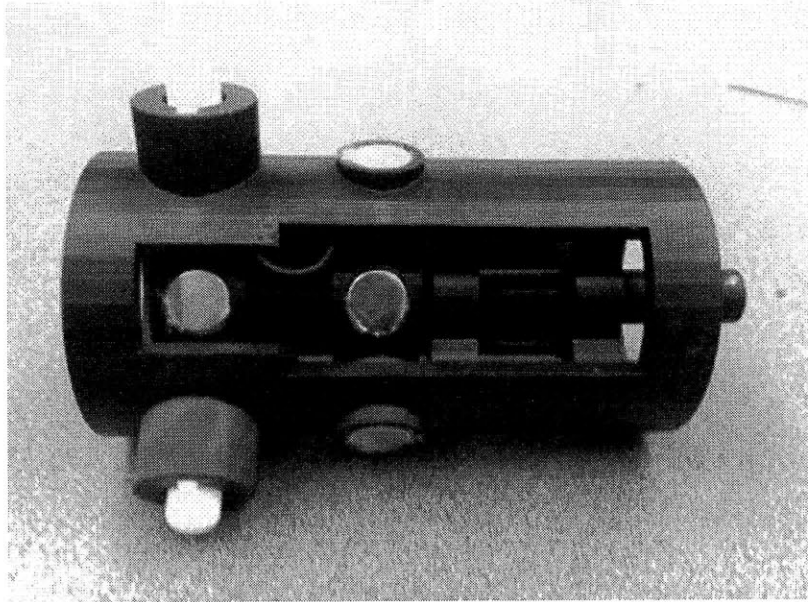


Figure 5-19: Prototype II with both front and rear stator/rotor pair.

Prototype I was built with only front stator/rotor pair and prototype II was built with both front and rear stator/rotor pair. This was done to effectively verify the torque cancelling effect that rear stator/rotor pair.



Experiments were done to measure the normal force and torque of the two prototype. The result showed the  $F_n$ - $\theta$  curve similar to the graph obtained from the simulation with both prototype producing similar amount of normal force for given angle  $\theta$ . However, while producing normal force of similar magnitude, the torque generated on the shaft by Prototype I was far greater than that of Prototype II. Prototype II did create a small torque but much smaller than that of Prototype I showing the effectiveness of the rear stator/rotor set in canceling out the undesirable torque.

## **5.6 Discussion and Future Work**

The major advantage of using the permanent magnet is that magnetic force varies with powers of 2-4 to distance and 4 to radius which gives large range of normal force possible in compact setting as well as applicability to various setting. Also the mechanism provides controllable normal force with servo motor controlling the angle that corresponds to desired normal force. Torque reduction by increase in number of stator poles and cancellation by pair stator/rotor magnets means no high torque servo motor is required for control which can lead to compactness and less energy consumption while servo motor does control action to adjust the angle. Torque cancellation gives possibility of friction in the servo motor gearing being sufficient to hold the rotor magnet in fixed angle meaning no energy is consumed while providing constant normal force.

The disadvantage of proposed mechanism is that cost of the magnet increase greatly as size increases. Also, normal force produced is highly sensitive to distance

meaning manufacturing error need to be minimized – requires precision machining and high cost. Moreover, the normal force cannot be exactly calculated analytically so need to experimentally obtain F-theta curve to use in control.

This mechanism can effectively be applied to produce normal force in in-pipe robots. Control the speed of the robot in the flow of fluidic pipe may also be possible by varying the friction force. There are more work needs to be done on the mechanism. To begin with, more precise experiment is needed setup to measure the torque and normal force to verify the results obtained from analysis. Verification using FEM software will also be of great help. Also, appropriate control algorithm may need to be developed in order to effectively use this mechanism in controlling the normal force to the desired value.

## **5.7 Conclusion**

In this chapter, a novel mechanism that generates controllable friction for in-pipe robot with minimal energy is presented. Detail of how permanent magnet is used in the mechanism to achieve the objective is discussed as well as important design parameters identified. Analysis of the mechanism is performed with appropriate modeling of the magnet and the relation between the design parameters and the performance is shown. Also built prototype of the mechanism is presented as a proof of concept.

# Chapter 6

## Propulsion Unit

### 6.1 Analysis of the Drag forces

For the selection and design of the propulsion unit for mobile robotic platform, it is necessary to first set a value of the thrust force that propulsion unit needs to produce. Since the thrust needed is directly related to the amount of drag force experienced by the robot, analysis of the drag force on the robotic platform becomes essential.

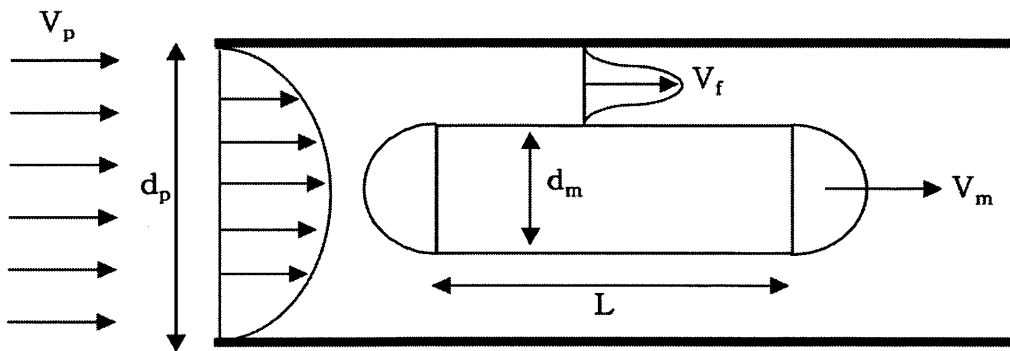


Figure 6-1: Schematic of the robotic platform inside a pipe with flow.

Figure 6-1 shows a schematic of the robotic platform inside a pipe with water flow. The relevant parameters that affect the drag force induced on the robot are labeled on the figure. Following is description of those parameters involved.

$d_p$  = Diameter of pipe

$d_m$  = Diameter of module

$V_f$  = Average velocity of pipe flow

$V_p$  = Average velocity between module & pipe

$L$  = Length of module

$V_m$  = Velocity of module

Assuming the pipe flow to be laminar and fully developed, a simple drag analysis can be performed. First, drag induced consist of pressure drag caused by the pressure difference in the front and rear part of the robot and friction drag that results from boundary layer formed along the surface of the robot.

$$Drag = D_{pressure} \oplus D_{friction} \quad (6.1)$$

The pressure drag can be calculated from Equation (6.2) with appropriate value of drag coefficient chosen for the shape of the robot.

$$D_{pressure} = \frac{1}{2} C_D \rho_{water} u_{\infty}^2 A \quad (6.2)$$

Here the following value of drag coefficient is used assuming the robot to have cylindrical body with front and rear end caps having hemispherical shape.

$$C_D = 0.2, \rho_{water} = 998kg/m^3$$

$$u_{\infty} = V_f \ominus V_m = \frac{V_p \times \pi(d_p/2)^2}{\pi((d_p/2)^2 \ominus (d_m/2)^2)} \ominus V_m \quad (6.3)$$

$$A = \text{frontal\_area} = \pi(d_m/2)^2$$

For the value of flow speed and frontal area, parameter values is put into Equation (6.3)

$$D_{friction} = \overline{\tau_w} \times \pi(d_m) \times L \quad (6.4)$$

$$(\overline{\tau_w} = \frac{1}{8} \rho (V_p \ominus V_m)^2 \times f, f \simeq f_{moody}(\text{Re}_{D_h}, \varepsilon / D_h), \varepsilon = 0)$$

In the similar manner, friction drag can be calculated from Equation (6.4) with friction factor based on the Reynolds number found from Moody's chart.

Now, with the Equation (6-2) and (6-4), drag force induced on the robotic platform can be calculated. The robot will experience maximum drag force when it is completely stationary inside a maximum flow speed (2 m/s). This corresponds to parameter values of  $V_p = 2\text{m/s}$ ,  $V_m = 0\text{m/s}$ ,  $d_p = 0.1\text{m}$ ,  $d_m = 0.06\text{m}$ ,  $L = 1\text{m}$ . Using these values, the maximum drag force is found as is as follow.

$$\text{Drag} = D_{pressure} \oplus D_{friction} = 2.76\text{N} \oplus 1.89\text{N} = 4.65\text{N} \simeq 5\text{N}$$

This result from simple analysis indicate that the propulsion unit to be designed must be able to produce at least 5N of force to either propel forward 2 m/s in stationary water or stop completely inside water flow of 2 m/s. The drag force found through the analysis is in good agreement with the CFD simulation result performed in previous literature. [1]

## 6.2 Candidates for Propulsion Unit

Several candidates were considered as possible propulsion unit to be used for the robotic platform. In this section, brief description of each that were considered is given.

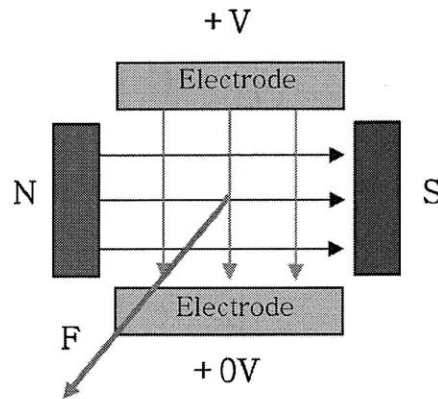


Figure 6-2: Schematic of magneto-hydrodynamic propulsion unit.

The first candidate considered is magneto-hydrodynamic propulsion unit. Figure 6-2 shows the schematic of one such unit. The basic principle behind magneto-hydrodynamic propulsion is the Lorentz force. An voltage difference is applied between two electrodes which are placed inside a magnetic field such that the electric fields cross perpendicular to the it. Due to the Lorentz effect, the medium of ions in between the electrodes experience a force that creates thrust.

The advantage of the magneto-hydrodynamic propulsion is that there is no moving part and it is silent. However, it produces significantly low thrust and also gas bubbles in the process. Further, to be used in robotic platform, the presence of magnetic field might interfere with the on-board electronics.

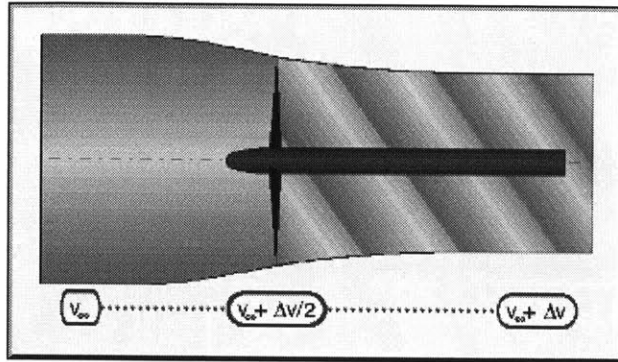


Figure 6-3: Schematic of propeller as propulsion unit.

Second candidate considered is propeller. Propeller works by adding the momentum to flow by shaft action and thereby generating thrust force by action and reaction. Propeller is an effective propulsion unit as it has several advantages over other propulsion unit. First, the amount of thrust produced is large. Also, the design is simple and low cost commercial parts are readily available. Further, propeller can be back propelled to generate energy from water flow for later use when energy harvesting unit is implemented. The drawbacks of propeller is that the it creates noise which might affect the performance of the sensor that detects the leak.

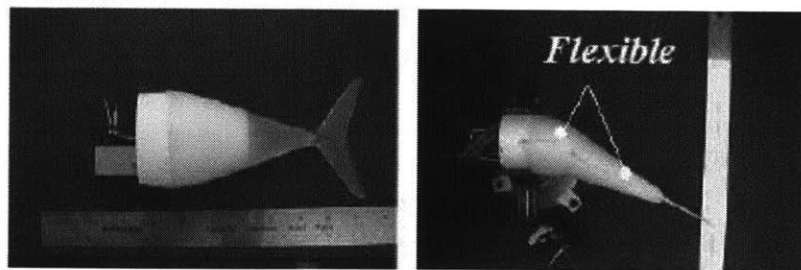


Figure 6-4: Fish-like motion propulsion.

Another possibility for propulsion unit is using flexible structured fin to generate thrust through undulated motion. Such fish like motion has pros in that the overall drag

coefficient of the robot can be reduced and there is no issue of sealing for propulsion components even at high pressure. Nevertheless, the thrust produced is not smooth, making precisely controlled thrust not possible and even the magnitude of thrust itself is relatively low.

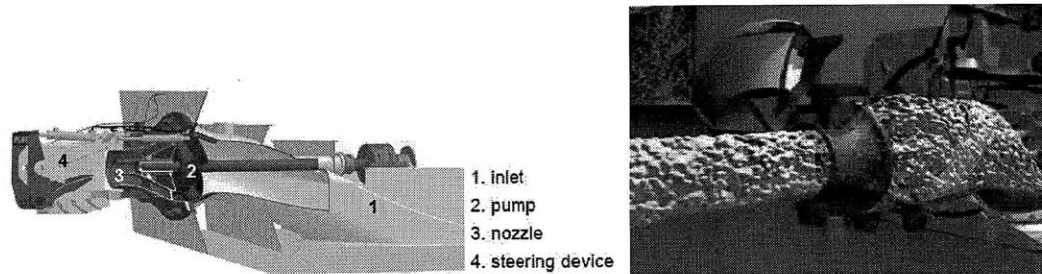


Figure 6-5: Water-jet propulsion unit.

Water-jet is another viable propulsion unit that can be used for the robotic platform. Water-jet works by compressing fluid through pump and then jetting out fluid through the nozzle to create thrust. It is in many ways similar to a propeller with difference being the fluid travels through closed nozzle rather than open-water as in the case of propeller.

### 6.3 Comparison of Different Propulsion Units

A comparison of different possible propulsion unit is carried out. The details of the thrust calculation will not be discussed in the thesis but the results is given in the Table 6-1. From the analysis comparing the different propulsion unit, propeller is chosen as the propulsion unit to be used in the robotic platform. The major reason for it is that propeller provides higher thrust compared to other units and at the same time simple to design and inexpensive commercial parts are readily available.



Propulsion Type	Maximum Thrust & Velocity	Advantages	Disadvantages
1. MHD	0.05 N 0.20 m/s	<ul style="list-style-type: none"> <li>- No moving part</li> <li>- Silent (good for sensing leak noise)</li> <li>- Can be used for both propulsion &amp; slow down</li> <li>- Fine control of thrust possible</li> </ul>	<ul style="list-style-type: none"> <li>- Very small thrust</li> <li>- Bubbles (hydrogen/oxygen) are generated</li> <li>- Magnetic field might interfere with on-board electronic devices</li> </ul>
2. Propeller	7.41 N 2.30 m/s	<ul style="list-style-type: none"> <li>- Thrust is large -&gt; can slow down &amp; stop completely at 2m/s flow</li> <li>- Can be back propelled to generate energy (while module is anchored) for recharging battery</li> <li>- Design is simple and low cost commercial parts readily available</li> </ul>	<ul style="list-style-type: none"> <li>- Create noise</li> <li>- Propeller can be damaged when hit on the wall of the pipe</li> <li>- Not novel</li> </ul>
3. Fish-like motion	Flexible fin 0.20N 0.38 m/s  Oscillating foil 2.5 N 1.30 m/s	<ul style="list-style-type: none"> <li>- Drag coefficient is not increased much compared to other propulsion type</li> <li>- Produce sufficient thrust to propel at reasonable speed</li> <li>- No issue of sealing under high pressure (flexible fin)</li> <li>- Design is simple (Oscillating foil)</li> </ul>	<ul style="list-style-type: none"> <li>- Cannot be used for slowing down</li> <li>- Thrust is not even (fluctuate over one cycle and only averaged thrust per cycle is available – may cause problem when trying to do speed control)</li> <li>- Propulsion system require certain length</li> </ul>
4. Synthetic Jet	0.25 N 0.43 m/s	<ul style="list-style-type: none"> <li>- Compact (doesn't take lot of space and propulsion system can be placed inside the module)</li> <li>- Only 1 moving part, minimal seal required</li> <li>- Drag coefficient is not increased at all</li> </ul>	<ul style="list-style-type: none"> <li>- Produce thrust only in one direction</li> <li>- Thrust is not even</li> </ul>

Table 6-1: Comparison of different propulsion units.

## 6.4 Conclusion

In this chapter, analysis of the drag force, brief description of the possible propulsion units and comparison of these units were presented. Only the selection process was completed so far and certainly further work needed to designing, building and testing

of the propulsion unit based on propeller. Once the propeller based propulsion unit is built and tested, the next step will be implementing controller to control the thrust for given purposes.

# Chapter 7

## Conclusion and Future Work

This thesis presented the design of mobile robotic platform that carries the necessary sensor and travels inside the water pipe systems. To begin with, experiments were carried out to investigate the suitability of using acoustic sensor to detect the leaks with favorable results obtained. Then design specification of the mobile robotic platform that will carry the sensor is discussed with brief description of each components of robot given. As components for the mobile robotic platform, a rigid-flexible robotic joint is developed that enables the robot to travel through bends and turns. Further, a novel braking mechanism using permanent magnet is presented. The mechanism results in a friction controllable leg that can be used to slow down and control the speed of robot in the presence of water flow. Finally, possible candidates for propulsion unit are discussed and evaluated.

For the follow up of the work, a propulsion unit needs to be designed, built and tested. The next step will be integrating together the components - rigid-flexible robotic joints, friction controllable legs and propulsion units to form a complete mobile robotic platform. Afterwards, a central processing controller needs to be implemented to

coordinate the working of each component to travel inside the water pipe.

Finally, the mobile robotic platform will incorporate necessary sensor, communication module, and power supply for the purpose of leak detection. The ultimate goal of mobile robotic platform is for the robot to be able to travel inside the network of water pipe systems autonomously, un-tethered with long hours of operation while detecting and sending out information about the leaks in the water pipe systems.

# Appendix A

## Friction Controlling Mechanism

### A.1 Using Magnetic Force

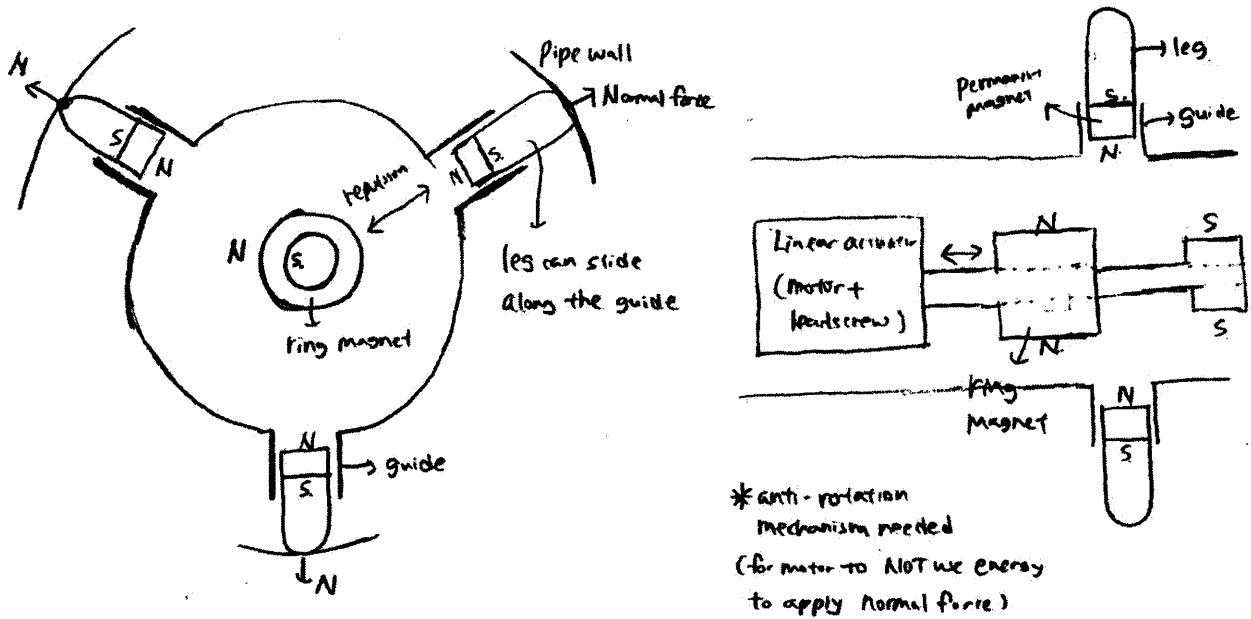


Figure A-1: Sketch of friction controlling mechanism using magnetic force.

Distance between the Ring magnet attached to the shaft of linear actuator and magnet attached to the end of each leg determines the normal force to be applied.

Additional ring magnet of opposite pole can be placed either in front or back of the main Ring magnet to act as retractor for the legs when linear actuator rotates to position it near the leg.

Anti-rotation mechanism for the linear actuator is needed to be able to apply normal force without consuming energy.

The magnetic force between the Ring magnet and magnet attached to each leg is proportional to  $1/\text{distance}^3$ , thus the normal force goes from almost zero to maximum in very small distance turn of linear actuator. This is good in the sense that linear actuator doesn't have to have long lead screw, but more precise linear position control is needed.

#### Advantage

- Very simple mechanism. Easy to make, can be compact, and no need for direct link between leg and actuator.
- Large range of force is achieved over small linear actuator distance.

#### Disadvantage

- Ring magnet might interfere with the magnetic field of the linear motor, thereby affecting its performance. (though highly unlikely due to  $1/\text{distance}^3$  factor)
- The legs might not be retracted fully due to volume occupied by ring magnet.

## A.2 Linkage or Cam Mechanism

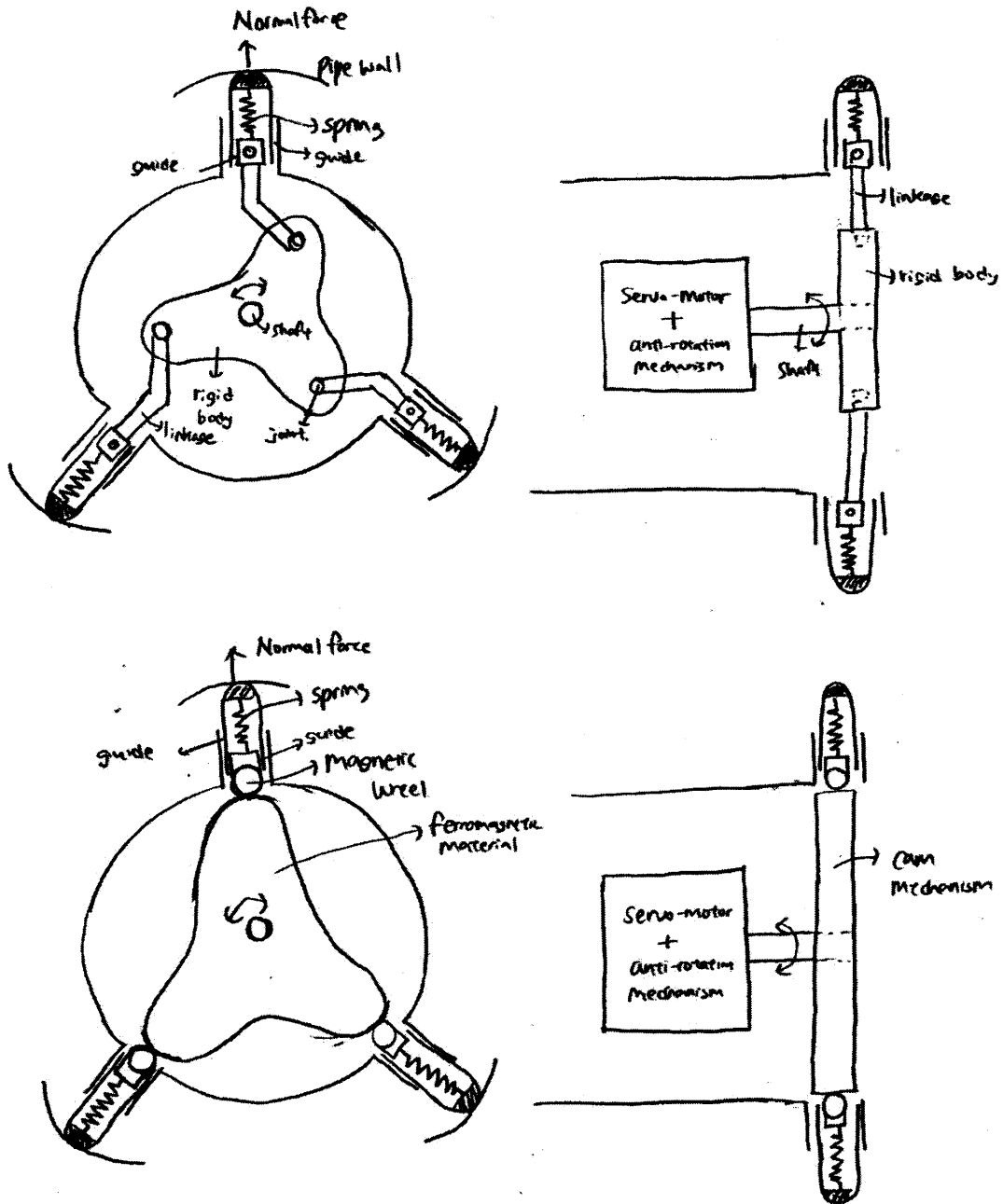


Figure A-2: Sketch of linkage and cam mechanism to control friction.

Motor (or servo-motor) is attached to a shaft. A linkage or cam attached to shaft is rotated. Depending on the angle of rotation, the spring attached to the leg can get compressed, providing normal force that is function of shaft angle (without spring, varying normal force cannot be applied without motor giving torque all the time. With spring, normal force becomes function of shaft angle, thus if anti-rotation mechanism holds shaft at certain angle without consuming energy, varying normal force can be applied with no motor torque applied.) If the shaft is turned other way, the leg can all together made to retract.

In case of cam, there is magnetic wheel attached at the end of each leg and the main rigid body attached to shaft is made of ferromagnetic material, so the leg will follow the contour of the main rigid body, thereby compressing spring to varying degree to produce varying normal force.

The main rigid body for both cam and linkage can be made with hollow inside to reduce the moment of inertia.

#### Advantages

- Using servo-motor can greatly reduce the complexity of problem.
- In case of cam, the contour profile can be selected to vary the angle – normal force relation.
- Legs can be fully retracted. Especially in the case of cam, there is plenty of space.



## Disadvantages

- Anti-rotation mechanism is needed. In case of linear actuator, anti-rotation mechanism might not be needed due to friction.
- Linkage requires links. Cam requires contact.

Cam mechanism is regarded as a better choice between the two for our purpose.

### A.2.1 Anti-Rotation Mechanism

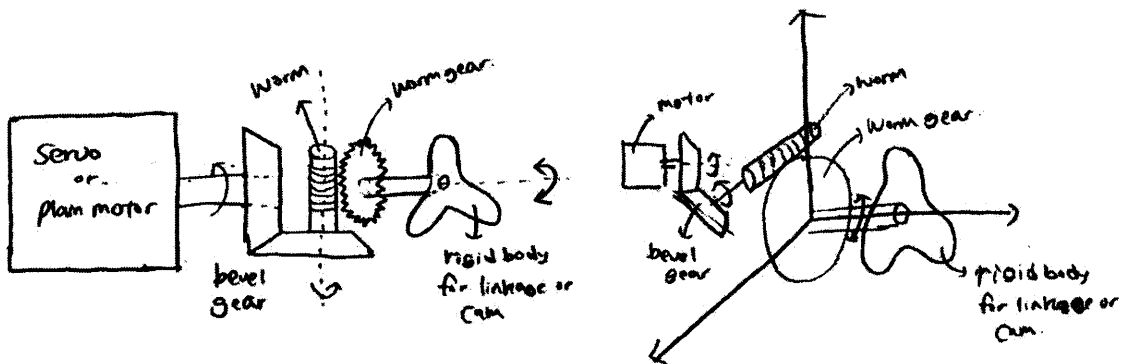


Figure A-3: Sketch of anti-rotation mechanism.

Plain motor can be attached to bevel gear then worm to provide the anti-rotation mechanism. The worm can rotate the worm gear, but due to friction, the worm gear cannot rotate worm. This provides the anti-rotation mechanism needed to hold the rigid body at certain angle without motor torque applied.

### A.3 Pneumatic / Hydraulic or Cable

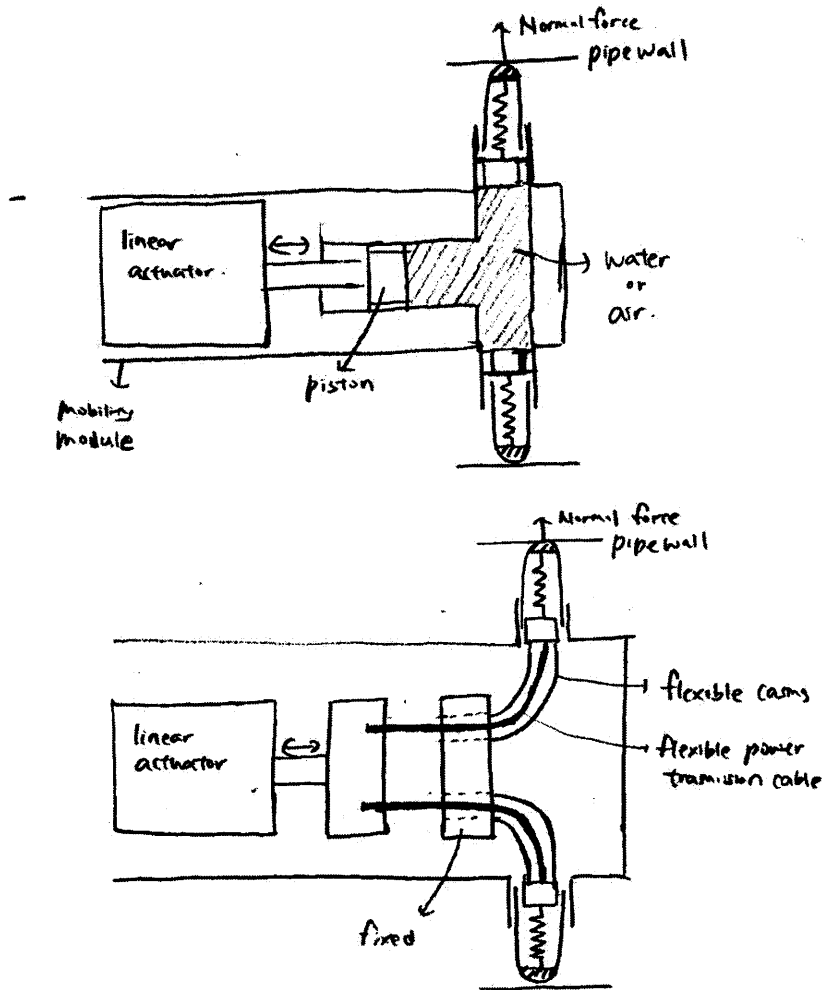


Figure A-4: Sketch of mechanism using pneumatic or cable to control friction.

Linear actuator drives either piston or flexible power transmission cable. Piston moves through pressurized air or water, thus transmitting force to the legs. The flexible power transmission cable is pushed or pulled to provide the needed normal force.

### Advantages

- Power transmission is can take place anywhere, so there is no restriction on where the legs can be.

### Disadvantages

- Cable needs longer length because it cannot directly transmit for perpendicularly. Piston also need certain length for it to move back and forth.
- Pneumatic/Hydraulic requires additional sealing, and also it might be undesirble to have pressurized water inside the robot for safety of electronics.



## Appendix B

### Magneto-hydrodynamic Propulsion Unit

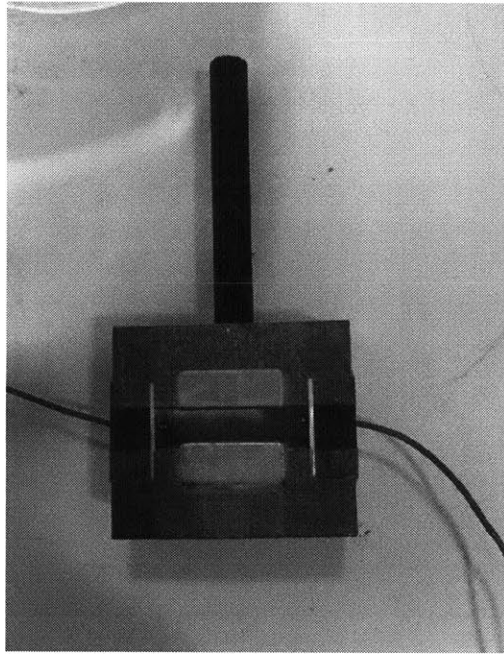


Figure B-1: Prototype of simple magneto-hydrodynamic propulsion unit.

For the purpose of verifying the possibility of using magneto-hydrodynamic unit as propulsion, a simple prototype has been built as shown in Figure B-1. The following design parameters affect the thrust produced by magneto-hydrodynamics and their respective values are listed in accordance with the working environment.

$V = \text{Voltage applied} = 20\text{V}$

$W = \text{width of electrode} = 2\pi r = 0.188\text{m}$

$L = \text{length of electrode} = \text{length of propulsion module} = 0.2\text{m}$

$B = \text{Magnetic field} = 1\text{T}$  (when NIB permanent magnet is used)

$k = \text{conductivity of electrolyte} = 0.002 \text{ S/m}$  (tap water)

$h = \text{distance between the electrode} = 0.01\text{m}$

Through simple analysis, thrust generated is given by

$$T = qv \times B = il \times B = \frac{V}{R} h \times B = \frac{VkWL}{h} h \times B = VkWLB = 0.01\text{N} \quad (\text{B.1})$$

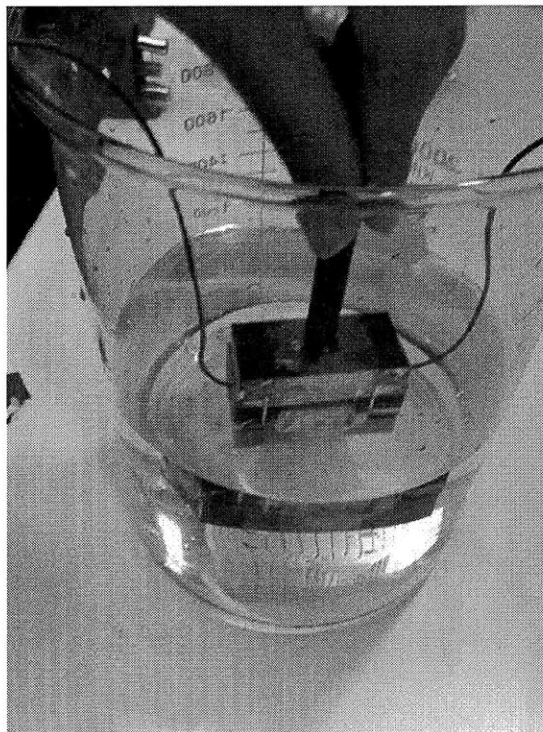


Figure B-2: Magneto-hydrodynamic unit tested inside salty water.

An experiment has been performed to verify the thrust produced by the magneto-hydrodynamic propulsion unit. Figure B-2 shows the unit submerged inside the salt water and Figure B-3 shows a photo of the unit taken while 20V of voltage was applied to the electrodes.

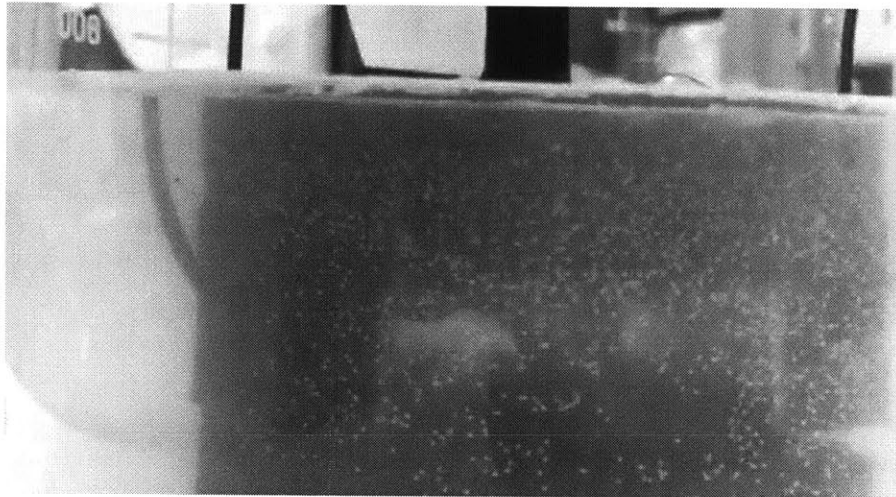


Figure B-3: Unit submerged inside salt water with 20V applied.

The magneto-hydrodynamic unit did produce some thrust as evidenced by the water being pushed out from the channel in between the two magnets. Nevertheless, as predicted by the theoretical calculation, the unit failed to produce any significant thrust that can be used to propel the robotic platform forward.

To augment the thrust, two design were considered that increased the magnetic field strength by packing the two magnets more closely and also enlarged the surface area of the electrodes. Figure B-4 shows the two designs that were considered.

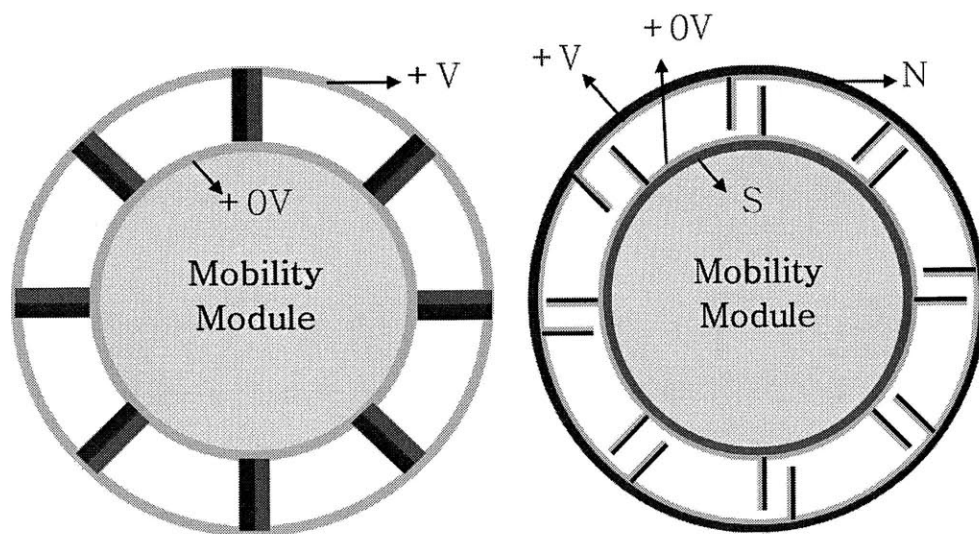


Figure B-4: Possible designs to augment the thrust.

However, even with the improved designs, thrust produced was not anywhere near what is needed of the robot traveling inside the water pipe. The main reason for it is the low value of conductivity of electrolyte of water. Water does not have enough ions for the Lorentz force effect to act upon and this value cannot be changed as the robot is designed to travel inside water pipe system.



# Bibliography

## Chapter 2

- [1] Brones, H., and Schaffhaussen, H., 1972, "European Methods of Leak Detection and Location," Pipeline Industry, pp. 50-66.
- [2] Hunaidi, O., and Chu, W. T., 1999, "Acoustical Characteristics of Leak Signals in Plastic Distribution Pipes," Applied Acoustics, Vol. 58, pp. 235-254.
- [3] Fuchs, H.V., and Riehle, R., 1991, "Ten years of experience with leak detection by acoustic signal analysis, *Applied Acoustics*, 33, pp. 1-19.
- [4] Bracken, M.; Hunaidi, O., 2005, "Practical aspects of acoustical leak location on plastic and large diameter pipe", Leakage 2005 Conference Proceedings, Halifax, N.S., pp. 448-452.
- [5] Hunaidi, O., Wang, A., and Guan, W., 2006, "A new system for locating leaks in urban water distribution pipes," Management of Environmental Quality: An International Journal, 17(4), pp. 450-466.
- [6] Bond, A., Mergelas, B., and Jones, C., 2004, "Pinpointing Leaks in Water Transmission Mains," Pipelines 146, 91.
- [7] Galleher, J., and W. Kurtz, D. W., 2008, "Evaluation of an Un-Tethered Free-Swimming Acoustic Leak Detection Technology," Journal of Water Resources

Planning and Management, Vol 58.

[8] Thompson, M., Chapman, C.J., Howison, S.D., and Ockendon, J.R., 2001, "Noise generation by water pipe leaks," 40th European Study Group with Industry, Keele.

[9] Muggleton, J. M., and Brennan, M. J., "Leak noise propagation and attenuation in submerged plastic water pipes," *Journal of Sound and Vibration*, vol. 278, pp. 527-537, 2004.

[10] Muggleton, J. M., et al., "Axisymmetric wave propagation in fluid-filled pipes: wavenumber measurements in in vacuo and buried pipes," *Journal of Sound and Vibration*, vol. 270, pp. 171-190, 2004.

[11] Gao, Y., et al., "A model of the correlation function of leak noise in buried plastic pipes," *Journal of Sound and Vibration*, vol. 277, pp. 133-148, 2004.

## **Chapter 3**

[1] J.M. Tur, W. Garthwaite, "Robotic Devices for Water Main In-Pipe Inspection: A Survey," in *Journal of Field Robotics*, 27(4),2010, pp.491-508.

## **Chapter 5**

[1] J.M. Tur, W. Garthwaite, "Robotic Devices for Water Main In-Pipe Inspection: A Survey," in *Journal of Field Robotics*, 27(4),2010, pp.491-508.

[2] M. Horodinca, I. Doroftei, E. Mignon, A. Preumont, "A Simple Architecture for In-Pipe Inspection Robots,"

- [3] S.G.Roh, H.R.Choi, "Differential-Drive In-Pipe Robot for Moving Inside Urban Gas Pipeline," in *IEEE Transactions on Robotics*, Vol. 21, No. 1, Feb. 2005.
- [4] M.M. Moghaddam<sup>1</sup> and A. Hadi, "Control and Guidance of a Pipe-Inspection Crawler (PIC)," in *International Symposium on Automation and Robotics in Construction*, Sep. 2005.
- [5] Y.S.Kwon, H.Lim, E.J.Jung, B.Y.Yi, "Design and Motion Planning of a Two-Moduled Indoor Pipeline Inspection Robot," in *IEEE International Conference on Robotics and Automation*, May, 2008.
- [6] C.Jun, Z. Deng, S.Y. Jiang, "Study of Locomotion Control Characteristics for Six-Wheel Driven In-Pipe Robot," in *IEEE International Conference on Robotics and Automation*, Aug. 2004.
- [7] S. Hirose, H. Ohno, T. Mitsui, K. Suyama, "Design of In-Pipe Inspection Vehicles for  $\phi 25$ ,  $\phi 50$ ,  $\phi 150$  Pipes," in *IEEE International Conference on Robotics and Automation*, May, 1999.
- [8] M.Komori and K. Suyama, "Inspection robots for gas pipelines of Tokyo Gas," in *Advanced Robotics*, Vol. 15, No. 3, 2001, pp. 365– 370.
- [9] M.Muramatsu, N.Namiki, R.Koyama, Y. Suga, "Autonomous Mobile Robot in Pipe for Piping Operations," in *International Conference on Intelligent Robots and Systems*, 2000.
- [10] D. Vokoun, M. Beleggia, L. Heller, and P. Sittner, "Magnetostatic interactions and forces between cylindrical permanent magnets," in *Journal of magnetism and Magnetic Materials*, 321, 2009, pp.3758-3763.

[11] J.S. Agashe and D.P. Arnold, "A study of scaling and geometry effects on the forces between cuboidal and cylindrical magnets using analytical force solutions," in *J. Phys. D: Appl. Phys.* 41, 2008, 105001.

## **Chapter 6**

[1] D.M. Chatzigeorgiou, "Analysis and Design of an In-Pipe System for Water Leak Detection", MS Thesis, MIT, 2010.